Evolution of cell size control is canalized towards adders or sizers by cell cycle structure and selective pressures

Félix Proulx-Giraldeau[1], Jan M. Skotheim[2,3] & Paul Francois[1]

[1]Department of Physics, McGill University, Canada
[2]Department of Biology, Stanford University, USA
[3]Chan Zuckerberg Biohub, San Francisco, USA

Abstract

Cell size is controlled to be within a specific range to support physiological function. To control their size, cells use diverse mechanisms ranging from 'sizers', in which differences in cell size are compensated for in a single cell division cycle, to 'adders', in which a constant amount of cell growth occurs in each cell cycle. This diversity raises the question why a particular cell would implement one rather than another mechanism? To address this question, we performed a series of simulations evolving cell size control networks. The size control mechanism that evolved was influenced by both cell cycle structure and specific selection pressures. Moreover, evolved networks recapitulated known size control properties of naturally occurring networks. If the mechanism is based on a G1 size control and an S/G2/M timer, as found for budding yeast and some human cells, adders likely evolve. But, if the G1 phase is significantly longer than the S/G2/M phase, as is often the case in mammalian cells *in vivo*, sizers become more likely. Sizers also evolve when the cell cycle structure is inverted so that G1 is a timer, while S/G2/M performs size control, as is the case for the fission yeast *S. pombe*. For some size control networks, cell size consistently decreases in each cycle until a burst of cell cycle inhibitor drives an extended G1 phase much like the cell division cycle of the green algae *Chlamydomonas*. That these size control networks evolved such self-organized criticality shows how the evolution of complex systems can drive the emergence of critical processes.

Introduction

Cell size is fundamental to cell physiology and function because it sets the scale of subcellular compartments, cellular biosynthetic capacity, metabolism, mechanical properties, surface-to-volume ratios, and molecular transport (Chan & Marshall, 2010; Ginzberg et al., 2015; Neurohr et al., 2019; Zatulovskiy & Skotheim, 2020). While different types of cells vary enormously in size to perform their functions, cells within a particular type are generally uniform in size indicating that cell growth may be accurately coupled to division and differentiation processes. On a

phenomenological level, there are many commonalities in how cells regulate their size even though the molecules controlling cell division vary across the tree of life with the most striking differences separating eukaryotes and bacteria. This extreme molecular diversity in the regulatory proteins raises the question as to what are the common features of the control systems that evolved to implement size control.

Most generally, cell size control can be viewed as a return map where the division size is a function of the cell size at birth. The examination of proliferating cells in laboratory conditions has revealed a variety of size control phenomena that can be characterized quantitatively by plotting the size of a cell at birth against the amount of mass added before it divides (Amir, 2014; Facchetti et al., 2017; Jun & Taheri-Araghi, 2015). A 'sizer' has a slope of -1 so that all variation in cell mass at birth is compensated for in one cell cycle, while an 'adder' has a slope of 0 so that each cell adds the same amount of mass during the cell cycle regardless of initial size. In the case of an adder, control is weaker so that multiple cell cycles are required for a particularly large or small cell to return to the average cell size. Importantly, the slope relating size at birth with the amount of growth in the cell cycle is a metric that quantifies the amount of size control occurring in a particular condition.

Studies of cell size control have revealed a diverse set of phenomena. Fission yeast and mouse epidermal stem cells exhibit 'sizers', and most bacteria, archaea, and cultured human cell lines exhibit behavior closer to adders (Cadart et al., 2018; Eun et al., 2018; Jun et al., 2018; Sveiczer et al., 1996; Westfall & Levin, 2017; Willis & Huang, 2017; Xie & Skotheim, 2020). Thus, while diverse size control behaviors have been observed, adders have been observed more often than sizers. This raises the question of why adders are more frequently observed if sizers, by definition, are more effective at controlling cell size?

To address the question of why adders are the most often observed form of cell size control, we used evolutionary algorithms (Holland, 1992) to identify commonalities between networks evolved to control cell size. Evolutionary algorithms are a class of machine learning techniques aiming at mimicking evolutionary processes (François & Hakim, 2004; François, 2014; Xiong et al., 2019; Crombach, 2021). Because of the nature of evolution, results of evolutionary computations are often more efficient and more creative than expected (Lehman et al., 2020). Furthermore, solutions found by evolutionary algorithms are more constrained by their evolutionary paths followed and present similar characteristics to biologically evolved systems (Schaerli et al., 2018). We start with a simple model of the cell cycle with a timer for an S/G2/M phase (Fig. 1) that we evolve to optimize homeostatic cell size control. We discovered that different control mechanisms could perform cell size control based on protein quantity or concentration. Simulations in which size control takes place in G1 phase converge towards an adder mechanism for the entire cell cycle and identified an active quantity sensing mechanism similar to dilution-based mechanisms previously identified experimentally (Chen et al., 2020; Qu et al., 2019; Schmoller et al., 2015). The relative durations of G1 and S/G2/M were important in determining size control properties. A relatively shorter S/G2/M phase favors sizer mechanisms, while longer S/G2/M phases favor adders. Moreover, inverting the model so that cell size rather than time controls the S/G2/M, like in fission yeast, results in more size-like control. Thus, we anticipate adders arise when cell size

is controlled at a point intermediate in the cell cycle, like the G1/S transition, while sizers will appear when cell size regulates a point later in the cell cycle, as is the case when G1 is proportionally longer, or control takes place at the transition to mitosis. While there is no one-to-one correspondence between a specific size control mechanism and a given evolutionary pressure, our work identifies clear evolutionary principles that shed light on the diverse cell size control phenomena previously observed experimentally.

Materials and Methods

Mathematical formalism

To model gene networks, we follow a standard ODE based formalism, where we simulate dynamics of the concentrations of proteins. We use Hill functions for transcriptional interactions, and standard mass action kinetics for protein-protein interactions. We also assume that all proteins are degraded at a constant rate. For most of the simulations presented in the paper, we use deterministic ODEs for simplicity. Importantly, cell-to-cell variability arises from the precise timing of cell cycle progression events (see below). This allows for a natural way to generate noise on cell volume that should then be compensated for by the evolved network. In the last part of the paper, we explicitly include Langevin noise for biochemical reactions that are modeled using a classical tau-leaping formalism (Gillespie, 2007). Thus, each biochemical reaction takes place with a Poisson rate that corresponds to the deterministic rate, to which we add one white Gaussian noise with a variance equal to that rate.

In general, there are two classes of mechanisms that cells use to control their size that can be separated in terms of whether cell division or cell growth *per se* is regulated by cell size. Note that in this work, we will use mass, size, and volume interchangeably. In the first class, it is crucial that the growth rate per unit mass of a cell depends on cell size so that cells further from the optimum cell size grow slower (Cadart et al., 2019; Ginzberg et al., 2018; Miettinen & Björklund, 2016; Nordholt et al., 2020; Tzur et al., 2009). Such slower growing cells are then outcompeted by cells closer to the optimum size even when divisions occur purely by chance (Conlon & Raff, 2003). While size-dependent growth mechanisms exist and do support size homeostasis, such mechanisms rely on inefficient growth in all the cells away from the optimum size. To avoid such inefficient growth, many types of cells use active size control mechanisms to accelerate progression through the cell cycle in larger cells (Zatulovskiy & Skotheim, 2020). In our simulations, we keep cell growth rates constant over a physiological range of cell sizes. This allows us to focus on the common features of the molecular networks in which increasing cell size drives changes in molecular activities to trigger cell division. We assume that cell volume V grows at a rate $\lambda(V) \times V$, so that growth is exponential when λ is a constant. Volume is divided by 2 at each division after which we follow one of the two daughter cells. The growth rate sets the time scale for the system dynamics as it defines the doubling time $\tau = ln\,(2)/\lambda$. Any interdivision time shorter than τ will see the cell volume shrink at the next generation while any interdivision time

larger than τ will see the cell volume grow. We also use the chemistry square bracket convention such that any protein X's *concentration* is denoted by $[X]$. Correspondingly, its *quantity* is denoted by X only and is defined as $X = [X] \times V$.

Volume influences protein dynamics in three ways. First, protein production rates are generally proportional to cell volume so that proteins reach and maintain a constant concentration that is independent of the cell volume (Chen et al., 2020; Elliott & McLaughlin, 1978; Newman et al., 2006; Swaffer et al., 2021). Thus, the only deterministic influence of volume on concentration dynamics is on the dilution rate, which is proportional to the cell growth rate $\lambda(V)$ (see details in Supplement). At cell division, we also assume that proteins are equally partitioned between the daughter cells, *i.e.*, the concentration is the same before and after division. The cell volume also contributes to stochastic effects, which are larger in smaller cells with fewer molecules. For stochastic simulations, we therefore include a multiplicative $\frac{1}{\sqrt{V}}$ contribution to the added Gaussian noise term (see more complete description in the Supplement). Note that we scale all our variables so that a concentration of one arbitrary unit corresponds roughly to 1000 proteins in a 100fL cell (Milo et al., 2010).

Evolutionary procedure

To evolve networks regulating cell size, we use the ***φ***-evo software (Henry et al., 2018) with a modified numerical integrator accounting for volume dynamics and volume dependencies as described above (Fig. 1B). ***φ***-evo simulates the Darwinian evolution of a population of gene networks. A network is encoded with the help of a bipartite graph connecting biochemical species (typically proteins) and interactions between them (we use a custom-made Python library). Networks are converted into an ensemble of stochastic differential equations using a Python to C interpreter. This code is then compiled and integrated on the fly to compute the behavior of the networks.

Each selection step in the algorithm is referred to as an *epoch* rather than the more commonly used term *generation* because we use the term generation to refer to cell divisions in the simulations. At each epoch of the algorithm, each gene network is simulated, and its fitness computed. Based on the fitness function(s) (see below), half of the networks are selected and duplicated, while the other half is discarded to maintain a constant population size. The duplicated networks are then randomly mutated. From the most to least probable, mutations consist in random changes of parameters of the network, random removal of interactions, and random additions of interactions or new proteins. All of this is easily made with our customized Python library encoding networks. For more details on technical aspects and implementations of the ***φ***-evo software, we refer the reader to (Henry et al., 2018).

Realistic evolutionary processes select for multiple phenotypes in parallel. While trade-offs between those phenotypes are non-trivial, it has been observed that phenotypes typically define an evolutionarily Pareto front (Shoval et al., 2012; Warmflash et al., 2012). We thus perform network selection using a Pareto mode (Warmflash et al., 2012), in which 2 distinct fitness

functions are computed. During the selection step, networks are first Pareto ranked. For example, consider two networks A and B and two fitness functions f^1 and f^2. f^1_A refers to the fitness of network A calculated with function f^1. Assuming fitness functions are to be maximized, we say network A Pareto-dominates network B if both $f^1_A > f^1_B$ and $f^2_A \geq f^2_B$. Rank 1 networks are networks which are not dominated by any other networks, Rank 2 networks are networks dominated only by Rank 1 networks, and Rank 3 networks are only dominated by Rank 1 and Rank 2 networks and so on. The algorithm then selects half of the population of Rank 1 networks using a fitness sharing algorithm to maximize population diversity (see details in (Warmflash et al., 2012)). One advantage of Pareto selection is the increased flexibility of the evolutionary process. Multiple fitness functions can provide different optimization paths in parameter space, which prevents the selection process from getting stuck in a local optimum of a single fitness function. We also perform a few simulations with only one fitness function, in which case networks are simply ranked based on their fitness.

We impose two evolutionary selection pressures in the form of two fitness functions. The first fitness function is simply the number of cell divisions during a long period, which we call N_{Div}. This is consistent with the classical definition of fitness as optimizing the number of offspring and is to be maximized by the algorithm. The second fitness function is the coefficient of variation of the volume distribution at birth for those N_{Div} generations, which we call CV_{Birth} and is to be minimized by the algorithm. This penalizes broad distributions of volume at birth, which are detrimental to cell size homeostasis. We also present results for additional fitness functions that we explored in the Supplement. These include a least-square residual function to minimize volume variation about a target size, and the fitted slope of the amount of volume added at each cycle to be minimized to drive models toward being a sizer.

Initial cell-cycle model

We initialize our network evolution simulations with a very simplified model of the cell-cycle. We model two independent phases of a symmetrically dividing cell, G1 and S/G2/M, separated by a commitment point at the end of G1 and division at the end of S/G2/M (Fig. 1A) (Chandler-Brown et al., 2017). We encode this cell cycle state information via a binary switch variable we call 'S/G2/M Switch' that is 0 in G1 and 1 in S/G2/M. In most simulations, we follow an inhibitor model (Heldt et al., 2018; Schmoller et al., 2015; Zatulovskiy et al., 2020) and assume that the probability of passing the G1/S transition is controlled by the *quantity* of a transcription regulator I. A lower quantity of this inhibitor I means a higher probability of a G1/S transition at the current time step of the simulation (Fig. S2). Like all other proteins, the quantity I is produced with a rate proportional to volume, degraded at a constant rate, diluted by cell growth, and equally partitioned between mother and daughter cells at division. We found that due to the volume scaling assumption, $[I]'s$ concentration alone was largely independent of volume and could not trigger a size-dependent G1/S transition, which is why we opted for the quantity of I instead (Fig. S3). Upon passing the G1/S transition, we assume cells are committed to division and there is a fixed time delay before they divide thus modeling S/G2/M as a timer. We fixed the timer duration to be roughly equal to 50% of the doubling time τ with some uniform noise such that G1 and S/G2/M

212 durations would be the same at equilibrium. Regulation of the quantity I during the cell cycle thus
213 controls the precise timing of the G1/S transition, but it is not always perfect since the transition
214 is probabilistic. This, along with the noise in S/G2/M timer duration, creates natural cell to cell
215 variability in volume that needs to be compensated for by the evolved mechanism. We note that
216 we initialized most of our simulations with one added interaction in which production of $[I]$ is
217 activated by the S/G2/M Switch variable to reset its concentration to a higher level before the next
218 generation. We initially ran simulations without this specific interaction but found that it
219 systematically appears in the initial stages of evolution simulations. We therefore included it in
220 the initial network to speed up our simulations. We refer the reader to the supplementary
221 information for more details.
222
223 Typical dynamics of this simple cell-cycle model are represented in Figure 1. These dynamics are
224 similar to models of cell cycles based on relaxation oscillators (Cross, 2003; Tsai et al., 2008).
225 The left and right slow branches correspond to G1 and S/G2/M, respectively, and the fast
226 horizontal branches represent G1/S and division. An intermediate fictitious nullcline is shown that
227 connects the typical concentration $[I]$ at G1/S and at division. Starting with cell birth, the system
228 goes down the left-G1 branch because of degradation, then jumps to the right-S/G2/M branch
229 below the threshold for the G1/S transition, stays there while moving up due to production by the
230 S/G2/M Switch, until it jumps back to the left branch at the end of the timer phase. We note that
231 there is no explicit volume control in this initial model since the only control comes from the
232 quantity of I which does not initially depend in any way on the volume. This initial quantity sensing
233 oscillator does not perform size control and instead results in unstable growth where size
234 deviations are amplified at each generation instead of being corrected (Fig. S3). Thus, the network
235 needs to evolve some other interactions and/or parameters to go beyond a simple G1 inhibitor
236 driven by production in S/G2/M to create a viable cell lineage.
237
238 We also ran evolutionary simulations with different cell cycle structures. For evolutionary
239 simulations where the G1/S transition was controlled by the concentration of $[I]$, we simply
240 change the probability to pass the G1/S transition to depend on concentration $[I]$ instead of its
241 quantity I. For evolutionary simulations with a cell cycle structure similar to that found in the fission
242 yeast *S. pombe*, we invert the cell cycle network structure. In this case, I quantity controls division
243 and the Switch is turned on for a fixed amount of time in G1. In terms of the relaxation oscillator,
244 this means that the left branch is now S/G2/M and the right branch is G1.
245
246

247 Results

248

249 Evolution of quantity-based size control mechanisms

250
251 To examine how networks controlling cell size could evolve, we ran an evolutionary algorithm that
252 optimizes both the number of divisions N_{Div} and the coefficient of variation of the size distribution
253 at birth CV_{Birth} (see Methods for algorithm details). Fig. 2A illustrates the behavior and results of

a typical evolutionary run. An almost linear Pareto front evolves as a function of the number of epochs, and eventually converges towards a flat horizontal line. This flat Pareto front corresponds to a set of networks able to control cell volume as indicated by the low CV_{Birth}. The optimal networks, at the right most end of this line, both maximize N_{Div} and minimize CV_{Birth}.

Evolution simulations are in part reproducible and most often lead to similar network topologies (Fig. 2B; Model A1 is a typical example). The network leading to this type of cell size control is very simple. One gene, R, is added to the seed network and is both repressed and titrated by I forming the network motif known as a Mixed Feedback Loop (François & Hakim, 2005). The mixed feedback loop network that reproducibly evolved is arguably the simplest network that can achieve size control within our formalism. This can be understood intuitively as follows. $[I]$ represses $[R]$, which is thus only produced when $[I]$ is low, *i.e.,* when the cell is close to the G1/S transition and in early S/G2/M. But, since the *quantity* $I = [I] \times V$ is fixed at G1/S by design, we get that the *concentration* $[I]$ is inversely proportional to the volume of the cell at the G1/S transition ($V_{G1/S}$) as shown in our simulations (Fig. 2C). This means that the synthesis rate and the concentration of $[R]$ become (linear) functions of the volume of $V_{G1/S}$ (Fig. 2C). This provides an explicit volume sensing mechanism via $[R]$ and allows the cell to retain memory of its volume at G1/S. Subsequently, titration of $[I]$ by $[R]$ provides negative feedback that regulates the total *quantity* of inhibitor I produced during S/G2/M, so that cells are now born with a *quantity* of inhibitor I that is independent of volume (Fig. 2D). Note that because of the timer in S/G2/M, volume at birth remains proportional to $V_{G1/S}$, the volume that set the scale for the concentration of $[R]$ at G1/S and throughout S/G2/M. After division, in the absence of production by the S/G2/M Switch, $[I]$ is further titrated in G1 by the remaining $[R]$ from the previous generation (still proportional to $V_{G1/S}$). This ensures that daughter cells reach the quantity threshold of G1/S earlier if they were born larger. When we examine the change in quantity of I as a function of time spent in G1 and of $V_{G1/S}$ we see the slope of these two quantities is volume-dependent. This confirms that the active titration mechanism is regulated by volume to provide a size control mechanism in G1 (Fig. 2E).

Our typical evolved size control networks, while relying on *quantity* sensing, are conceptually similar to the budding yeast network relying on *concentration* sensing of the cell cycle inhibitor Whi5 since there is a constant quantity of I present right after division (just like Whi5). In budding yeast, the Whi5 protein is passively diluted in G1 to increase the stochastic rate of progression through the G1/S transition. The time spent in G1 depends on the initial concentration of Whi5 at birth, which scales as 1/V, to promote a sizer mechanism. Here, the concentration of $[I]$ at birth scales as 1/V, but so does the threshold concentration of $[I]$ regulating the G1/S transition. This is precisely why an active titration mechanism is required to obtain G1 size control in our setup. Such homeostatic control ensures cell size returns to its steady state distribution following an artificial perturbation as soon as a volume deviation is detected at G1/S (Fig. 2F). When we plot the amount of volume added ΔV for different phases of the cell cycle as a function of the initial volume at the beginning of these phases, we find an approximate adder over the whole cycle that results from weak sizer in G1 followed by a timer in S/G2/M as has been found in budding yeast (Chandler-Brown et al., 2017; Soifer et al., 2016) (Fig. 2G).

While we chose one simple model to illustrate the control mechanism common to our set of evolved networks (Model A1 shown in Fig. 2B), other evolved networks were more elaborate but illustrated a similar principle. For example, Model A2 contains extra interactions for the volume sensing gene R, where $[R]$ is repressed by the S/G2/M Switch (meaning its production is completely shut down in S/G2/M). Furthermore, $[R]$ represses the synthesis of $[I]$, adding another layer of repression to promote size control (Fig. 2H). If we perturb cell size to examine the dynamics of the return to steady state and look at the added volume during the cell cycle, we again see overall a weak adder behavior similar to that found in Model A1 (Fig. 2I-J).

Quantifying size control

To study the mechanisms implicated in cell size control, we modify the control at G1/S and introduce the control volume V_C. This control variable is independent from the biochemical network and is maintained fixed allowing us to disconnect the actual cell volume from the biochemical network and by forcing the G1/S transition to be triggered once $I_C = [I] \times V_C$ is low enough. We then numerically integrate the differential equations of the model and measure the period $T(V_C)$ of the simulated cell-cycle for this control volume. This allows us to break the size feedback system and distinguish its input, $V_{G1/S}$, from its output, the induced cycle period T (Angeli et al., 2004). We compute $T(V_C)$ for Models A1 and A2 and compare their responses with the analytical curves of the archetypical timer, adder, and sizer (Fig. 3A,C). Those curves intersect at the point where the induced period is exactly equal to the population doubling time (ln(2)/λ), which defines the equilibrium volume V_{eq} achieved by our cell size control network. Examination of the size control in different cell cycle phases indicates the contributions of G1 and S/G2/M to the overall system behavior (Fig. 3B,D). We note that we later examine statistics of ensembles of evolved models but that Models A1 and A2 are both typical examples of evolved feedback-based models.

Quantifying precisely how the cell cycle period depends on the control volume at G1/S allows us to see that the $T(V_C)$ for Model A1 overlaps with the theoretical adder curve over a broad range of volumes. In contrast, Model A2 behaves as a sizer for volumes smaller than the equilibrium volume. However, at higher volumes it behaves more like an adder/timer similar to Model A1. Model A2's equilibrium is thus 'tuned' by evolution to be in a regime corresponding to the minimum of the ΔV_{Cycle} curve extrapolated from the $T(V_C)$ as shown in Fig. 3D, precisely when the system transits from a sizer at small volumes to an adder-like behavior at higher volumes. Similar behavior was observed experimentally in budding yeast (see Fig. 4C in (Chandler-Brown et al., 2017)). Thus, both Models A1 and A2 approximate an adder near the equilibrium size, but their behavior differs further from equilibrium where for smaller volumes, Model A1 is still an adder while Model A2 is a sizer.

Modulating cell cycle structural constraints selects for adders or sizers

So far, our evolutionary algorithm selects networks that implement adders rather than sizers near the equilibrium size. This is surprising because sizers are in principle be better able to control cell size and reduce the CV of the size distribution at birth, which is one of our fitness functions. That

adders are more frequently observed in nature than sizers (Cadart et al., 2018; Eun et al., 2018; Jun et al., 2018; Westfall & Levin, 2017; Willis & Huang, 2017; Zatulovskiy & Skotheim, 2020), is consistent with our evolution simulations, but adds to the mystery as to why this takes place.

To gain insight into the underlying reason for the prevalence of adders, we considered what might be exceptional in the cases where sizers occur. The best studied, and highly accurate sizer, is found in the fission yeast *S. pombe* (Fantes, 1977; Sveiczer et al., 1996). In contrast to budding yeast and human cells, where the size control takes place largely in G1 phase, fission yeast exerts size control later in the cell cycle at the G2/M transition. That size control took place later in the cell cycle in fission yeast suggested that this structural feature of its cell cycle might be responsible for its stronger size control. To test this, we inverted our seed network so that the G1 phase was a timer, while cell size control could evolve in S/G2/M (see Methods above). We compare these results to the evolutionary simulations starting with the 'control' seed network with G1 size control and an S/G2/M timer (Fig. 2).

To determine how the seed network structure influences the subsequent evolution of cell size control, we performed 120 independent evolutionary simulations for the two network structures initialized with the Model A1 topology and parameters (Fig. 4). 60 simulations were performed using Pareto optimization and another 60 simulations were performed using individual fitness optimization based on the number of cell divisions N_{Div}. For each simulation's fittest model after 500 epochs, we calculate the CV of the volume distribution at birth, CV_{Birth}, and the slope of the linear fit of the volume added in the entire cell cycle as a function of the cell size at birth, Slope ΔV_{Cycle} (we remind the reader that a slope of -1 corresponds to a sizer, 0 to an adder, and 1 to a timer). Model A1's initial CV_{Birth} and Slope ΔV_{Cycle} before evolution are indicated by the dashed black line. In the control experiment where G1 is a sizer and S/G2/M is a timer, most evolutionary simulations with two fitness functions (Pareto) yield models close to the adder regime with a low CV_{Birth}. However, when only the number of divisions (N_{Div}) is used as a fitness, the evolutionary simulations are closer to the sizer regime, albeit with a slightly higher CV_{Birth} (Fig. 4A, Welch's *t*-test $p < 10^{-4}$). When the cell cycle structure is inverted so that G1 is a timer and S/G2/M is a sizer like it is in the fission yeast *S. pombe*, we found that more sizer-like networks evolve than in the control experiment (Fig. 4B, Welch's *t*-test on agglomerated data $p = 0.03$). This shows that having a network structure like the fission yeast *S. pombe* promotes sizers, while having the size control portion of the cell cycle earlier, as in the budding yeast *S. cerevisiae*, promotes adders. Thus, performing simulations using cell cycle network structures of these two yeasts results in the evolution of size control mechanisms that reflects those that are naturally occurring.

The general notion that having cell size control in G1 results in adder-like mechanisms, while control later in the cell cycle results in more sizer-like mechanisms fits most observations of human cell lines grown in culture, budding yeast, and fission yeast. However, a recent study examining mouse epidermal stem cells growing and dividing in the skin found both a strong sizer and that this sizer was largely due to the size-dependent regulation of G1 (Mesa et al., 2018; Xie & Skotheim, 2020). This raised the question as to how a network performing size control in G1 could result in a sizer for the entire cell cycle. One important difference between mammalian cells grown in culture and the mouse epidermal stem cells growing in an animal (*in vivo*) is the change

in the relative durations of the G1 and S/G2/M phases of the cell cycle. While the S/G2/M phase of the cell cycle is similar in duration in cultured cells and the epidermal stem cells *in vivo* at ~12 hours, the G1 phase extends ~5-fold from ~10 hours in culture to ~50 hours *in vivo* (Cadart et al., 2018; Xie & Skotheim, 2020). This suggests the hypothesis that the overall size control behavior can be dominated by the relatively longer cell cycle phase, as is likely the case for the G1 phase of epidermal stem cells. To test this hypothesis, we performed evolutionary simulations with size control in G1 and a timer in S/G2/M but where we changed the duration of the S/G2/M timer phases of the cell cycle to be significantly shorter or longer than the G1 phase at equilibrium. When a timer in S/G2/M is relatively shorter compared to G1, we generally see more sizer-like behavior can evolve (Fig. 4C, Welch's *t*-test on agglomerated data $p = 4 \times 10^{-3}$), while when it is relatively longer, we see more adder-like or even timer-like behavior (Fig. 4D, Welch's *t*-test on agglomerated data $p < 10^{-4}$).

Taken together, our simulations show how the structural features of the cell cycle are important for determining what type of size control ultimately evolves. G1 control is more conducive to the evolution of adders, while G2 control is more conducive to sizers. Moreover, size control can be dominated by the cell cycle phase of longest duration and is modulated by the specific selection criteria.

A two-step evolutionary pathway for cell size control

From our series of evolution simulations, we found a somewhat paradoxical inverse correlation between the added volume slope quantifying the degree of size control (sizer vs. adder) and the CV_{Birth} (Fig. 4B-C). This was surprising because it means that there is a broader distribution of volumes in the sizer regime where control should be more effective in theory. To better understand this inverted correlation between Slope ΔV_{Cycle} and CV_{Birth}, we revisited our evolutionary simulations to examine the evolutionary pathways through which the networks progressed through the simulated epochs.

A typical evolutionary pathway for a Pareto simulation of the *S. pombe*-like network structure presented in Fig. 4B is shown in detail in Fig. 5. Here, Model A1 topology is conserved throughout evolution although individual parameter values change. In the early stages of the evolution (epoch 650), we typically see dynamics where small cell size triggers an overshoot to a large cell size, which is then reduced through a series of rapid divisions (Fig. 5A). Because of this small-size-triggered overshoot, the system behaves more like a sizer when the average behavior is analyzed (Fig. 5B). However, the high degree of variability in the cell cycles also leads to a broad distribution of volumes (Fig. 5C). The variability in volume is attenuated in later epochs where there are fewer and smaller volume overshoots triggered by small cell size (Fig. 5 D-I). Since small cell size no longer triggers a dramatic amount of cell growth, the slope of ΔV_{Cycle} is increased and the system converges towards a weak adder in which the distribution of volume at birth is more Gaussian and the CV_{Birth} is lower (Fig. 5H-I). Taken together, these analyses suggest a two-step evolutionary pathway, consistent with the evolutionary dynamics first seen in Fig. 2A. First, a strong sizer mechanism evolves, but because of noise in the system, small variations in volume lead to a dramatic overcorrection and overshoot of the target volume. The variability in volume

429 produced by this overshoot is then reduced by attenuating the strength of the size control
430 response. Indeed, the overall weaker size control allows the system to respond more mildly to
431 size deviations and yields a lower CV_{Birth} overall, which we select for. Thus, selecting for a smaller
432 CV_{Birth}, *i.e.*, better size control, can end up selecting for adders rather than sizers. This
433 paradoxical result is consistent with the fact that when we select only for the number of cell
434 divisions (N_{Div}), one sees that more sizer-like behavior can evolve (Fig. 4A-C).
435

436 ## Fluctuation sensing and the evolution of self-organized criticality

437

438 One of the main features of smaller cells is that they have fewer proteins and mRNA. If some
439 aspects of protein synthesis and degradation are subject to Poisson fluctuations, we expect such
440 fluctuations to produce larger concentration fluctuations in smaller cells. For example, if we
441 consider the synthesis and degradation of the quantity of a generic protein as a Poisson process
442 with parameter $\frac{\rho V}{\delta}$, where ρ is the synthesis rate in number of proteins per unit of time for a
443 reference volume of 1, *V* is the volume, and δ is the degradation rate. The average concentration
444 of this protein will be $\frac{\rho}{\delta}$, which is independent of the cell volume V as expected from the production
445 rate scaling. However, following the Bienaymé formula, the variance in the concentration is $\frac{\rho V}{\delta} \times$
446 $\frac{1}{V^2} = \frac{\rho}{\delta V}$ (Fig. 6A), which decreases with volume. This result makes intuitive sense because bigger
447 cells have to produce more proteins to keep concentrations constant, so that the fluctuations in
448 the relative number of proteins (and thus concentration) are smaller. Thus, if the cell could sense
449 the size of *concentration fluctuations* in some way, it would be able to harness the cell size-
450 dependence of such stochastic Poisson fluctuations to regulate cell division and control cell size.
451

452 To test if we can evolve networks that control cell size through sensing Poissonian fluctuations,
453 we first initialized our simulation with a network similar to that shown in Fig. 1C, but with an added
454 activating gene A that can activate the production of the I inhibitor. We then ran evolutionary
455 simulations using the cell cycle structure of a sizer controlling G1 and timer in S/G2/M, but where
456 the G1/S transition is regulated by the *concentration* $[I]$ instead of its *quantity.* We also used
457 Pareto fitness optimization of N_{Div} and of CV_{Birth}. Importantly, we use the stochastic version of
458 our equations with the molecular noise modeled using a Langevin noise term with a variance
459 inversely proportional to the volume as explained above. We then extracted the most fit network
460 and optimized it further using Pareto optimization of N_{Div} and of the ΔV_{Cycle} slope to push the
461 models towards the sizer regime. The most fit network of those combined evolutionary
462 simulations is presented in Fig. 6B and demonstrates that we can indeed evolve fluctuation-based
463 cell size control (Model B).
464

465 The mechanism for size control that evolved based on size-dependent fluctuation sensing is
466 remarkably similar to what we observed for models without size-dependent fluctuations (Fig. 5A).
467 For large volumes, the cycle has a constant period which corresponds to approximately 85% of
468 the doubling time τ. This ensures that in the high-volume regime, the system shrinks over time.
469 When the volume is small however, fluctuations allow the concentration $[A]$ to cross the threshold

of the highly non-linear transcriptional activation of $[I]$ by $[A]$. This results in a massive increase of $[I]$ that needs to be degraded to progress further into the cell cycle. Thus, the low volume regime occasionally leads to a considerable increase in G1 length and a correspondingly very large cell at division. These very large cells then reliably and deterministically re-enter multiple, rapid cell cycles with short G1 until the cell is small again and the concentration fluctuations again become large enough to trigger the activation of $[I]$ by $[A]$. This mechanism thus appears very similar to the sizer mechanism observed in other quantity sensing simulations shown in Fig. 5. However, here the mechanism is based only on size-dependent fluctuations in protein concentration and the overall behavior is closer to an adder (Fig. 6E).

The system dynamics that evolved to perform fluctuation-based cell size control produce volume distributions that are long-tailed due to the stochastic occurrence of occasional exceptionally long G1 phases. Interestingly, the probability distribution of cell cycle durations follows a power law (Fig. 6F), which is due to the very broad distributions of G1 duration at lower cell volumes. A more controlled analysis specifying the initial conditions showed that cell cycles get increasingly long, and their distributions widen with decreasing control volume V_C (Fig. 6G). Such non-Gaussianity is the hallmark of critical behavior, suggesting that the evolution of fluctuation-based cell size control is based on self-organized criticality (SOC). SOC is defined as a system where an order parameter feeds back on a control parameter (Sornette et al., 1995; Vidiella et al., 2021). The canonical example of SOC is the sandpile to which grains of sand are added on top. As the sand accumulates, the slope steepens, and the angle of the pile (control parameter) increases. Eventually, this triggers avalanches (order parameter) that feedback to dramatically reduce the angle of the pile. This ensures that the system dynamically tunes itself at the critical value of the angle of the pile where avalanches can occur.

We conclude that our evolved size control network exhibits SOC based on several observations. Starting from a high volume, multiple divisions at a rate faster than it takes to double the biomass reduce cell volume V just like the addition of grains of sand gradually increase the slope of the pile. Then, for small enough volumes, bursts of $[A]$ drive an extended G1 that greatly increases cell size, which, like the sandpile avalanches, resets the system's control parameter (volume of the cell or angle of the sandpile). Interestingly, evolution tuned the system to be near a bifurcation (Fig. 6H). If we consider the deterministic regime, in which the fluctuations in $[A]$ are small, the cycle is unperturbed and oscillates with a period roughly equal to 85% of the doubling time (Fig. 6I). In contrast, if we consider the noisy regime, in which the fluctuations in $[A]$ are large, the cycle disappears, and the system stays locked in a prolonged G1 state with a high value of $[A]/[I]$ which is akin to a bifurcation destroying the cycle (Fig. 6H). This bifurcation takes place because the position of the G1 attractor for $[I]$ becomes larger with increasing $[A]$ and eventually overcomes the concentration required to induce the stochastic G1/S transition (Fig. 6H inset). Then, the system remains stuck in a state where G1/S cannot be triggered, and cells effectively exit the cycle. As growth occurs, noise dies down and so does the position of the G1 attractor, eventually becoming smaller than the $[I]$ concentration required to induce the G1/S transition which allows cells to re-enter the cell cycle. Thus, the system is critical from a dynamical systems standpoint and also fits the general observation that SOC systems tune themselves to be right at the point where the order parameter is non zero, but infinitesimal (Sornette et al., 1995). In our case, the

bifurcation corresponds exactly to the point where $[A]$ can sufficiently activate the production of $[I]$ to prevent the G1/S transition.

Discussion

The last decade saw an explosion of time lapse microscopy studies measuring how cells control their size. These studies revealed diverse phenomena that are characterized by the correlation between cell size at birth and cell size at division. Size control ranged from sizers, where the size at division is uncorrelated from the size at birth, to adders, which add a constant volume in each cell division cycle, to timers, whose cell cycle duration is size-independent (Cadart et al., 2018; Eun et al., 2018; Jun et al., 2018; Willis & Huang, 2017; Wood & Nurse, 2015; Zatulovskiy & Skotheim, 2020). The presence of these diverse phenomena raises the question as to why the underlying control networks evolve one rather than another type of cell size control?

To explore the evolution of cell size control networks subject to distinct selection pressures, we used computational evolution simulations. We initially examined the evolution of a seed cell cycle model consisting of G1 and S/G2/M phases of similar duration, where the G1 phase was free to evolve size-dependence, but the S/G2/M phase was constrained as a timer. Our simulations reliably evolved a control mechanism based on a Mixed Feedback Loop (François & Hakim, 2005) (Fig. 2). This network is centered on a cell cycle regulator (I) that inhibits the G1/S transition in proportion to its quantity. $[I]$ is titrated away into an inactive complex by an increasing amount of another protein $[R]$ that is synthesized in proportion to cell size. This results in a size-dependent decrease in the effective cell cycle inhibitor (free $[I]$). Thus, our evolved network implements an effective dilution of a cell cycle inhibitor that is conceptually similar to the well-described inhibitor dilution models of budding yeast, human cells, and *Arabidopsis* plants (D'Ario et al., 2021; Schmoller et al., 2015; Xie & Skotheim, 2020; Zatulovskiy et al., 2020). We note that we did not allow the synthesis of our proteins, such as $[I]$, to be size-independent as has been found for budding yeast (Chen et al., 2020; Schmoller et al., 2015; Swaffer et al., 2021) as this could result in a one-step implementation of cell size control through the pure dilution of a cell cycle inhibitor. It is therefore interesting that given the constraint that all proteins be made in proportion to cell size, the network still evolved an effective 'dilution' of the active form of the cell cycle inhibitor molecule $[I]$.

Our evolution simulations gave insight into factors that bias evolution towards sizer or adder type control mechanisms (Fig. 4). First, it is worth noting that our evolution simulations were not deterministic. There was no one-to-one correspondence between a given evolutionary pressure and any one specific cell size control mechanism. Rather, our claims represent an average behavior observed over the course of many simulations. In the selection of a size controlling G1 network followed by a timer in S/G2/M as described above, we observed a prevalence of adders that is consistent with the prevalence of adders reported in the literature. While fewer in number, sizers have also been observed. That the most accurate sizers have been observed in the fission yeast *S. pombe* (Fantes, 1977; Sveiczer et al., 1996; Wood & Nurse, 2015), and that this organism performs cell size control at G2/M rather than at G1/S led us to explore the effect of cell cycle

structure on the evolution of cell size control. We found that controlling cell size later in the cycle in S/G2/M biases evolution away from adders and towards sizers. In retrospect, this result can be rationalized since any size deviations incurred earlier during the timer period can be compensated for by the end of the cycle with the sizer. However, when the order is inverted, any size deviations escaping a G1 control mechanism would only be amplified by exponential volume growth during the S/G2/M timer period. A second recent case exhibiting sizer control was found in mouse epidermal stem cells, which exhibit a greatly elongated G1 phase and a relatively short S/G2/M phase (Mesa et al., 2018; Xie & Skotheim, 2020). We found that if we increased the relative duration of G1 in our simulations by shortening the S/G2/M timer, we also see a bias towards sizer control. Taken together, these simulations suggest the principle that having size-dependent transitions later in the cell cycle selects for sizers, while having such transitions earlier selects for adders.

In addition to identifying cell cycle structural features that canalize evolution towards sizers and adders as described above, we also observed an intriguing mechanism relying on Poissonian molecular fluctuations. In this case, small cells would trigger an abnormally long G1 that would result in very large cells that decrease in size through a series of rapid cell divisions. This type of size control is reminiscent of that found in the green algae *Chlamydomonas* where a series of rapid, size-reducing cell divisions cease when cells go below a target size (Heldt et al., 2020). In our case, small size results in larger concentration fluctuations due to Poisson noise in the number of molecules. These concentration fluctuations, when large enough, are then able to trigger a burst of G1/S inhibitor that leads to an extended G1 phase and massive cell size growth before another series of rapid cell divisions is initiated (Fig. 6). Due to the occasional massive volume growth at small birth sizes, there is a strong inverse correlation between the birth size and the amount of cell growth in the cell cycle. This mechanism thus results in a weak adder that displays high variability in cell size. However, the system still performs statistical size control over many generations. Intriguingly, this size control mechanism exhibits hallmarks of self-organized criticality (SOC). Just like adding grains of sand to a pile eventually triggers avalanches, the consistent decrease of cell size in the rapid division cycles eventually triggers a greatly extended G1 phase. To our knowledge, this is the first example where self-organized criticality is obtained in artificially evolved models of gene networks performing a well-defined function and is consistent with the idea that evolution of complex systems can favor the emergence of critical processes.

Acknowledgements

We thank Rodrigo Reyes-Lamothe, Nicolas E. Buchler, and Lucas Fuentes Valenzuela for helpful comments on the manuscript. JS was supported by the NIH (R35 GM134858), PF was supported by Natural Sciences and Engineering Research Council of Canada (NSERC) , Discovery Grant Program, FPG was supported by a Fonds de Recherche du Québec Nature et Technologies (FRQNT) Doctoral scholarship (B2X) and by a Natural Sciences and Engineering Research Council of Canada (NSERC) Doctoral Canada Graduate Scholarship (CGS-D).

Conflict of interest

The authors declare no conflict of interest.

References

Amir, A. (2014). Cell Size Regulation in Bacteria. *Physical Review Letters*, *112*(20), 208102. https://doi.org/10.1103/PhysRevLett.112.208102

Angeli, D., Ferrell, J. E., & Sontag, E. D. (2004). Detection of multistability, bifurcations, and hysteresis in a large class of biological positive-feedback systems. *Proceedings of the National Academy of Sciences*, *101*(7), 1822-1827. https://doi.org/10.1073/pnas.0308265100

Barr, A. R., Cooper, S., Heldt, F. S., Butera, F., Stoy, H., Mansfeld, J., Novák, B., & Bakal, C. (2017). DNA damage during S-phase mediates the proliferation-quiescence decision in the subsequent G1 via p21 expression. *Nature Communications*, *8*(1), 14728. https://doi.org/10.1038/ncomms14728

Cadart, C., Monnier, S., Grilli, J., Sáez, P. J., Srivastava, N., Attia, R., Terriac, E., Baum, B., Cosentino-Lagomarsino, M., & Piel, M. (2018). Size control in mammalian cells involves modulation of both growth rate and cell cycle duration. *Nature Communications*, *9*(1), 3275. https://doi.org/10.1038/s41467-018-05393-0

Cadart, C., Venkova, L., Recho, P., Lagomarsino, M. C., & Piel, M. (2019). The physics of cell-size regulation across timescales. *Nature Physics*, *15*(10), 993-1004. https://doi.org/10.1038/s41567-019-0629-y

Chan, Y.-H. M., & Marshall, W. F. (2010). Scaling properties of cell and organelle size. *Organogenesis*, *6*(2), 88-96. https://doi.org/10.4161/org.6.2.11464

Chandler-Brown, D., Schmoller, K. M., Winetraub, Y., & Skotheim, J. M. (2017). The Adder Phenomenon Emerges from Independent Control of Pre- and Post-Start Phases of the Budding Yeast Cell Cycle. *Current Biology*, *27*(18), 2774-2783.e3. https://doi.org/10.1016/j.cub.2017.08.015

Chen, Y., Zhao, G., Zahumensky, J., Honey, S., & Futcher, B. (2020). Differential Scaling of

630 Gene Expression with Cell Size May Explain Size Control in Budding Yeast. *Molecular*
631 *Cell*, *78*(2), 359-370.e6. https://doi.org/10.1016/j.molcel.2020.03.012
632 Conlon, I., & Raff, M. (2003). Differences in the way a mammalian cell and yeast cells
633 coordinate cell growth and cell-cycle progression. *Journal of Biology*, *2*(1), 7.
634 https://doi.org/10.1186/1475-4924-2-7
635 Crombach, A. (Éd.). (2021). *Evolutionary systems biology : Advances, questions, and*
636 *opportunities* (Second edition). Springer.
637 Cross, F. R. (2003). Two Redundant Oscillatory Mechanisms in the Yeast Cell Cycle.
638 *Developmental Cell*, *4*(5), 741-752. https://doi.org/10.1016/S1534-5807(03)00119-9
639 D'Ario, M., Tavares, R., Schiessl, K., Desvoyes, B., Gutierrez, C., Howard, M., & Sablowski, R.
640 (2021). Cell size controlled in plants using DNA content as an internal scale. *Science*.
641 https://doi.org/10.1126/science.abb4348
642 Elliott, G. & McLaughlin, C. S. (1978). Rate of macromolecular synthesis through the cell cycle
643 of the yeast Saccharomyces cerevisiae. *Proc. Natl. Acad. Sci. USA*, *75*, pp. 4384-4388.
644 https://doi.org/10.1073/pnas.75.9.4384
645 Eun, Y.-J., Ho, P.-Y., Kim, M., LaRussa, S., Robert, L., Renner, L. D., Schmid, A., Garner, E., &
646 Amir, A. (2018). Archaeal cells share common size control with bacteria despite noisier
647 growth and division. *Nature Microbiology*, *3*(2), 148-154. https://doi.org/10.1038/s41564-
648 017-0082-6
649 Facchetti, G., Chang, F., & Howard, M. (2017). Controlling cell size through sizer mechanisms.
650 *Current Opinion in Systems Biology*, *5*, 86-92.
651 https://doi.org/10.1016/j.coisb.2017.08.010
652 Fantes, P. A. (1977). Control of cell size and cycle time in Schizosaccharomyces pombe.
653 *Journal of Cell Science*, *24*(1), 51-67. https://doi.org/10.1242/jcs.24.1.51
654 François, P. (2014). Evolving phenotypic networks in silico. *Seminars in Cell & Developmental*
655 *Biology*, *35*, 90-97. https://doi.org/10.1016/j.semcdb.2014.06.012

François, P., & Hakim, V. (2004). Design of genetic networks with specified functions by evolution in silico. *Proceedings of the National Academy of Sciences*, *101*(2), 580-585.

François, P., & Hakim, V. (2005). Core genetic module : The mixed feedback loop. *Physical Review E*, *72*(3), 031908. https://doi.org/10.1103/PhysRevE.72.031908

Gillespie, D. T. (2007). Stochastic simulation of chemical kinetics. *Annual Review of Physical Chemistry*, *58*, 35–55. https://doi.org/10.1146/annurev.physchem.58.032806.104637

Ginzberg, M. B., Chang, N., D'Souza, H., Patel, N., Kafri, R., & Kirschner, M. W. (2018). Cell size sensing in animal cells coordinates anabolic growth rates and cell cycle progression to maintain cell size uniformity. *eLife*, *7*, e26957. https://doi.org/10.7554/eLife.26957

Ginzberg, M. B., Kafri, R., & Kirschner, M. (2015). On being the right (cell) size. *Science*, *348*(6236), 1245075. https://doi.org/10.1126/science.1245075

Heldt, F. S., Lunstone, R., Tyson, J. J., & Novák, B. (2018). Dilution and titration of cell-cycle regulators may control cell size in budding yeast. *PLOS Computational Biology*, *14*(10), e1006548. https://doi.org/10.1371/journal.pcbi.1006548

Heldt, F. S., Tyson, J. J., Cross, F. R., & Novák, B. (2020). A Single Light-Responsive Sizer Can Control Multiple-Fission Cycles in Chlamydomonas. *Current Biology*, *30*(4), 634-644.e7. https://doi.org/10.1016/j.cub.2019.12.026

Henry, A., Hemery, M., & François, P. (2018). φ-evo : A program to evolve phenotypic models of biological networks. *PLOS Computational Biology*, *14*(6), e1006244. https://doi.org/10.1371/journal.pcbi.1006244

Holland, J. H. (1992). *Adaptation in natural and artificial systems : An introductory analysis with applications to biology, control, and artificial intelligence* (1st MIT Press ed). MIT Press.

Jun, S., Si, F., Pugatch, R., & Scott, M. (2018). Fundamental principles in bacterial physiology—history, recent progress, and the future with focus on cell size control : A review. *Reports on Progress in Physics*, *81*(5), 056601. https://doi.org/10.1088/1361-6633/aaa628

Jun, S., & Taheri-Araghi, S. (2015). Cell-size maintenance : Universal strategy revealed. *Trends*

682 *in Microbiology*, *23*(1), 4-6. https://doi.org/10.1016/j.tim.2014.12.001
683 Lehman, J., Clune, J., Misevic, D., Adami, C., Altenberg, L., Beaulieu, J., Bentley, P. J.,
684 Bernard, S., Beslon, G., Bryson, D. M., Cheney, N., Chrabaszcz, P., Cully, A., Doncieux,
685 S., Dyer, F. C., Ellefsen, K. O., Feldt, R., Fischer, S., Forrest, S., … Yosinski, J. (2020).
686 The Surprising Creativity of Digital Evolution : A Collection of Anecdotes from the
687 Evolutionary Computation and Artificial Life Research Communities. *Artificial Life*, *26*(2),
688 274-306. https://doi.org/10.1162/artl_a_00319
689 Mesa, K. R., Kawaguchi, K., Cockburn, K., Gonzalez, D., Boucher, J., Xin, T., Klein, A. M., &
690 Greco, V. (2018). Homeostatic Epidermal Stem Cell Self-Renewal Is Driven by Local
691 Differentiation. *Cell Stem Cell*, *23*(5), 677-686.e4.
692 https://doi.org/10.1016/j.stem.2018.09.005
693 Miettinen, T. P., & Björklund, M. (2016). Cellular Allometry of Mitochondrial Functionality
694 Establishes the Optimal Cell Size. *Developmental Cell*, *39*(3), 370-382.
695 https://doi.org/10.1016/j.devcel.2016.09.004
696 Milo, R., Jorgensen, P., Moran, U., Weber, G., & Springer, M. (2010). BioNumbers—The
697 database of key numbers in molecular and cell biology. *Nucleic Acids Research*,
698 *38*(suppl_1), D750-D753. https://doi.org/10.1093/nar/gkp889
699 Mora, T., & Bialek, W. (2011). Are biological systems poised at criticality? *Journal of Statistical*
700 *Physics*, *144*(2), 268-302. https://doi.org/10.1007/s10955-011-0229-4
701 Neurohr, G. E., Terry, R. L., Lengefeld, J., Bonney, M., Brittingham, G. P., Moretto, F.,
702 Miettinen, T. P., Vaites, L. P., Soares, L. M., Paulo, J. A., Harper, J. W., Buratowski, S.,
703 Manalis, S., van Werven, F. J., Holt, L. J., & Amon, A. (2019). Excessive Cell Growth
704 Causes Cytoplasm Dilution And Contributes to Senescence. *Cell*, *176*(5), 1083-
705 1097.e18. https://doi.org/10.1016/j.cell.2019.01.018
706 Newman, J. R. S., Ghaemmaghami, S., Ihmels, J., Breslow, D. K., Noble, M., DeRisi, J. L., &
707 Weissman, J. S. (2006). Single-cell proteomic analysis of S. cerevisiae reveals the

architecture of biological noise. *Nature*, *441*(7095), 840-846. https://doi.org/10.1038/nature04785

Nordholt, N., van Heerden, J. H., & Bruggeman, F. J. (2020). Biphasic Cell-Size and Growth-Rate Homeostasis by Single Bacillus subtilis Cells. *Current Biology*, *30*(12), 2238-2247.e5. https://doi.org/10.1016/j.cub.2020.04.030

Qu, Y., Jiang, J., Liu, X., Wei, P., Yang, X., & Tang, C. (2019). Cell Cycle Inhibitor Whi5 Records Environmental Information to Coordinate Growth and Division in Yeast. *Cell Reports*, *29*(4), 987-994.e5. https://doi.org/10.1016/j.celrep.2019.09.030

Schaerli, Y., Jiménez, A., Duarte, J. M., Mihajlovic, L., Renggli, J., Isalan, M., Sharpe, J., & Wagner, A. (2018). Synthetic circuits reveal how mechanisms of gene regulatory networks constrain evolution. *Molecular Systems Biology*, *14*(9). https://doi.org/10.15252/msb.20178102

Schmoller, K. M., Turner, J. J., Kõivomägi, M., & Skotheim, J. M. (2015). Dilution of the cell cycle inhibitor Whi5 controls budding-yeast cell size. *Nature*, *526*(7572), 268-272. https://doi.org/10.1038/nature14908

Shoval, O., Sheftel, H., Shinar, G., Hart, Y., Ramote, O., Mayo, A., Dekel, E., Kavanagh, K., & Alon, U. (2012). Evolutionary Trade-Offs, Pareto Optimality, and the Geometry of Phenotype Space. *Science*, *336*(6085), 1157-1160. https://doi.org/10.1126/science.1217405

Soifer, I., Robert, L., & Amir, A. (2016). Single-Cell Analysis of Growth in Budding Yeast and Bacteria Reveals a Common Size Regulation Strategy. *Current Biology: CB*, *26*(3), 356-361. https://doi.org/10.1016/j.cub.2015.11.067

Sornette, D., Johansen, A., & Dornic, I. (1995). Mapping Self-Organized Criticality onto Criticality. *Journal de Physique I*, *5*(3), 325-335. https://doi.org/10.1051/jp1:1995129

Spencer, S. L., Cappell, S. D., Tsai, F.-C., Overton, K. W., Wang, C. L., & Meyer, T. (2013). The proliferation-quiescence decision is controlled by a bifurcation in CDK2 activity at mitotic

exit. *Cell*, *155*(2), 369–383. https://doi.org/10.1016/j.cell.2013.08.062

Sveiczer, A., Novak, B., & Mitchison, J. M. (1996). The size control of fission yeast revisited. *Journal of Cell Science*, *109*(12), 2947-2957. https://doi.org/10.1242/jcs.109.12.2947

Swaffer, M. P., Kim, J., Chandler-Brown, D., Langhinrichs, M., Marinov, G. K., Greenleaf, W. J., Kundaje, A., Schmoller, K. M., & Skotheim, J. M. (2021). Transcriptional and chromatin-based partitioning mechanisms uncouple protein scaling from cell size. *Molecular Cell*, *81*(23), 4861-4875.e7. https://doi.org/10.1016/j.molcel.2021.10.007

Tsai, T. Y.-C., Choi, Y. S., Ma, W., Pomerening, J. R., Tang, C., & Ferrell, J. E. (2008). Robust, Tunable Biological Oscillations from Interlinked Positive and Negative Feedback Loops. *Science (New York, N.Y.)*, *321*(5885), 126-129. https://doi.org/10.1126/science.1156951

Tzur, A., Kafri, R., LeBleu, V. S., Lahav, G., & Kirschner, M. W. (2009). Cell Growth and Size Homeostasis in Proliferating Animal Cells. *Science*, *325*(5937), 167-171. https://doi.org/10.1126/science.1174294

Vidiella, B., Guillamon, A., Sardanyés, J., Maull, V., Pla, J., Conde, N., & Solé, R. (2021). Engineering self-organized criticality in living cells. *Nature Communications*, *12*(1), 4415. https://doi.org/10.1038/s41467-021-24695-4

Warmflash, A., Francois, P., & Siggia, E. D. (2012). Pareto evolution of gene networks : An algorithm to optimize multiple fitness objectives. *Physical Biology*, *9*(5), 056001. https://doi.org/10.1088/1478-3975/9/5/056001

Westfall, C. S., & Levin, P. A. (2017). Bacterial Cell Size : Multifactorial and Multifaceted. *Annual Review of Microbiology*, *71*, 499-517. https://doi.org/10.1146/annurev-micro-090816-093803

Willis, L., & Huang, K. C. (2017). Sizing up the bacterial cell cycle. *Nature Reviews Microbiology*, *15*(10), 606-620. https://doi.org/10.1038/nrmicro.2017.79

Wood, E., & Nurse, P. (2015). Sizing up to divide : Mitotic cell-size control in fission yeast. *Annual Review of Cell and Developmental Biology*, *31*, 11-29.

https://doi.org/10.1146/annurev-cellbio-100814-125601

Xie, S., & Skotheim, J. M. (2020). A G1 Sizer Coordinates Growth and Division in the Mouse Epidermis. *Current Biology*, *30*(5), 916-924.e2. https://doi.org/10.1016/j.cub.2019.12.062

Xiong, K., Lancaster, A. K., Siegal, M. L., & Masel, J. (2019). Feed-forward regulation adaptively evolves via dynamics rather than topology when there is intrinsic noise. *Nature Communications*, *10*(1), 2418. https://doi.org/10.1038/s41467-019-10388-6

Zatulovskiy, E., & Skotheim, J. M. (2020). On the Molecular Mechanisms Regulating Animal Cell Size Homeostasis. *Trends in Genetics*, *36*(5), 360-372. https://doi.org/10.1016/j.tig.2020.01.011

Zatulovskiy, E., Zhang, S., Berenson, D. F., Topacio, B. R., & Skotheim, J. M. (2020). Cell growth dilutes the cell cycle inhibitor Rb to trigger cell division. *Science*, *369*(6502), 466-471. https://doi.org/10.1126/science.aaz6213

Figures

Figure 1

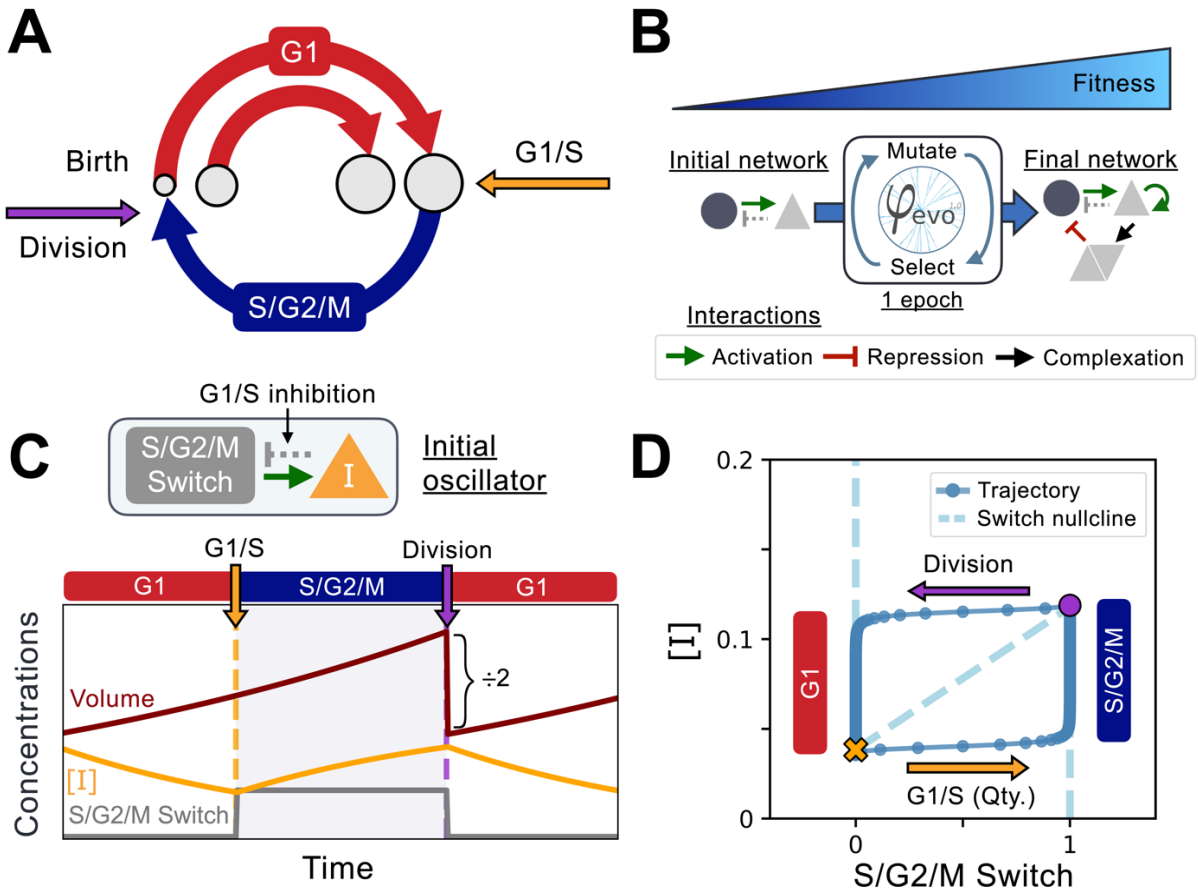

Figure 1 - Implementation of the cell cycle seed network and evolution algorithm.
A) Schematic representation of the coupling between cell size and cell cycle progression. The transition between G1 (red) and S phases of the cell cycle at the G1/S transition (orange) can evolve to depend on cell size, while the duration of the S/G2/M (blue) phase is independent of size. Cell division takes place instantaneously following mitosis (purple).
B) Schematic representation of the φ-evo algorithm implementation. The network generating tool takes an initial network topology as its starting point for evolution as well as a user-defined fitness function. φ-evo then goes through successive epochs of mutation and selection to extract a final optimized network. At each selection step, the fittest half of the networks are retained and duplicated for evolution in the subsequent epoch. Permitted interactions allowed by φ-evo include transcriptional activation (green arrow), transcriptional repression (red arrow) and protein-protein interactions responsible for complex formation (black arrow).
C) Schematic of our seed network topology implementing a simplified relaxation oscillator. Cell cycle state (G1 or S/G2/M) is encoded via a binary switch called *'S/G2/M Switch'* that is 0 in G1 and 1 in S/G2/M. Transition between G1 and S is controlled by the quantity of an inhibitor of the G1/S transition that we call I. The lower the quantity I, the higher the chance of progression through the G1/S transition. This interaction is represented as the grey arrow in the network

topology. After progressing through G1/S, cells enter S/G2/M which we model as a pure timer of fixed duration with some uniform noise. Cell volume grows exponentially and is divided symmetrically following mitosis. We then follow one of the daughter cells and disregard the other one.

D) Phase-space representation of the initial relaxation oscillator. The X-coordinate shows the S/G2/M Switch variable, and the Y-coordinate shows the concentration of $[I]$. The oscillator runs counterclockwise with the left branch (x=0) corresponding to G1 and the right branch (x=1) corresponding to S/G2/M. The G1/S transition and division events are instantaneous in our simulations but are smoothly represented here for visualization purposes. From these transitions, we can extract the approximate shape of the $[I]$ nullcline that we plot under the oscillator with a dashed line. We note that the position of the G1/S transition in phase-space will vary as a function of the volume of the cell as it depends on the *quantity* of $I = [I] \times V$ rather than its *concentration* $[I]$.

Figure 2

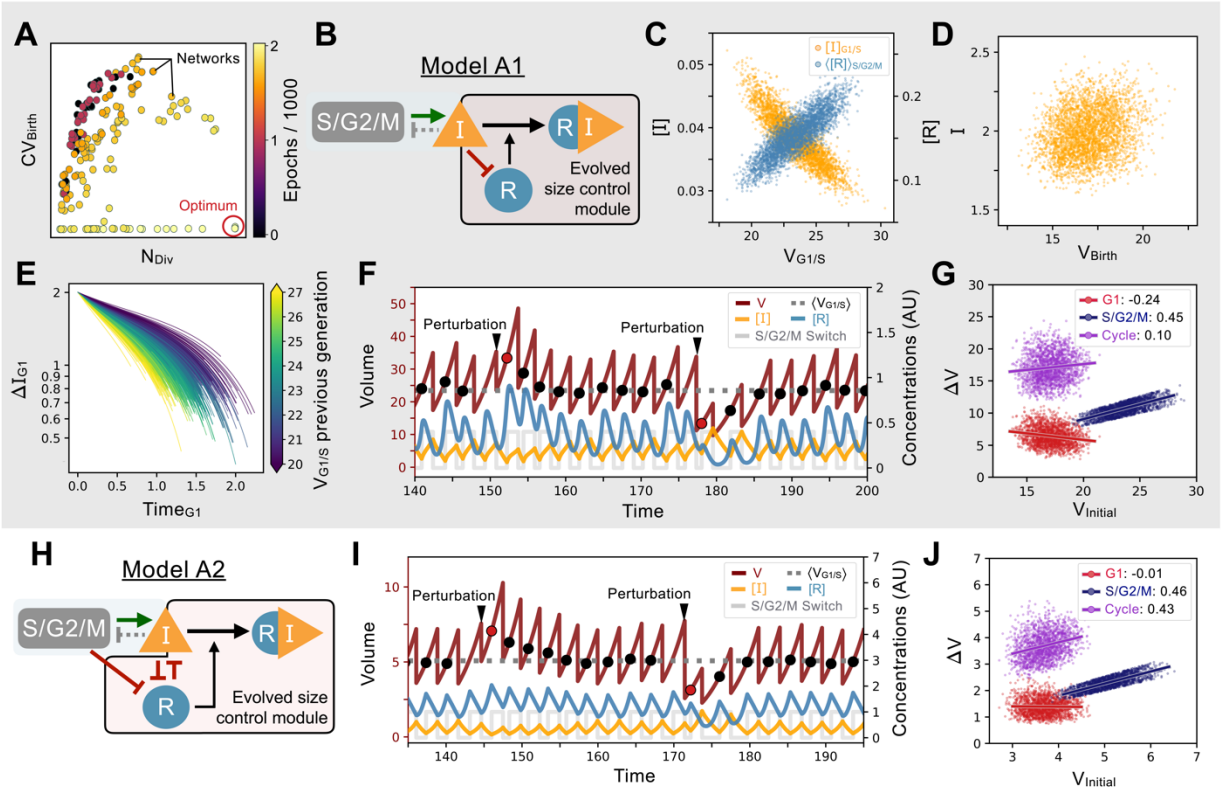

Figure 2 - Evolution of feedback-based size control:

A) Typical 2D fitness trajectory for an evolutionary run showing the number of divisions of a cell lineage during a time interval of fixed length (N_{Div}, X-coordinate) and the coefficient of variation of the volume distribution at birth (CV_{Birth}, Y-coordinate). Optimal model behavior is located in the bottom right corner of the figure where networks produce cell lineages with many offspring and strong size control. Individual networks are dots color coded by their epoch within the evolutionary trajectory.

B) Core network topology of the evolved Model A1 network that employs a feedback-based mechanism described in detail in panels C-F.

C) Concentration of $[I]$ at the G1/S transition (Y-coordinate, left axis, orange) and average concentration of the repressor protein $[R]$ in S/G2/M (Y-coordinate, right axis, light blue) as a function of the volume of the cell at G1/S (X-coordinate), *i.e.*, the beginning of S phase. We see here that $[R]$ acts as a direct size sensor of the volume at G1/S.

D) *Quantity* of inhibitor I at birth as a function of volume of the cell at birth, which is independent of size due to titration by $[R]$ during S/G2/M.

E) Trajectories of quantity of inhibitor I in G1 as a function of time. Trajectories are color coded as a function of the volume at G1/S during the previous generation's cell cycle. For visualization purposes, trajectories are offset vertically to all begin at the average *quantity* of I at birth (t=0) shown to be on average independent of volume in panel D. Larger cell volumes lead to greater titration of $[I]$ in G1 by $[R]$. In turn, this ensures that G1 duration of the daughter cell cycle is shorter, which underpins the size control mechanism.

F) Characteristic dynamics of Model A1. Trajectories of $[I]$, $[R]$ and S/G2/M Switch are rescaled with arbitrary units (AU) for visualization purposes. Circles indicate volume at G1/S. Extrinsic perturbations are applied to the model by temporarily changing the division ratios which kicks the system out of equilibrium at the subsequent cycle. The volume relaxation back to its homeostatic value takes ~2-3 generations regardless of if the perturbation is applied towards higher or lower volumes.

G) Amount of volume added (ΔV) in G1 (red), S/G2/M (dark blue), and over the whole cycle (purple) as a function of their initial volume at the beginning of these phases, *i.e.,* birth for G1 and cycle, and G1/S for S/G2/M, with the slope of linear fits indicated in legend. Slope of 1 corresponds to a Timer, slope of -1 to a Sizer and slope of 0 to an Adder.

H) Network topology of Model A2, a second evolved network that is similar to Model A1 albeit with different kinetic parameters and 2 additional interactions.

I) Typical dynamics of Model A2. Concentrations are rescaled with arbitrary units as in panel F.

J) Amount of volume added for different periods of the cell cycle for Model A2.

Figure 3

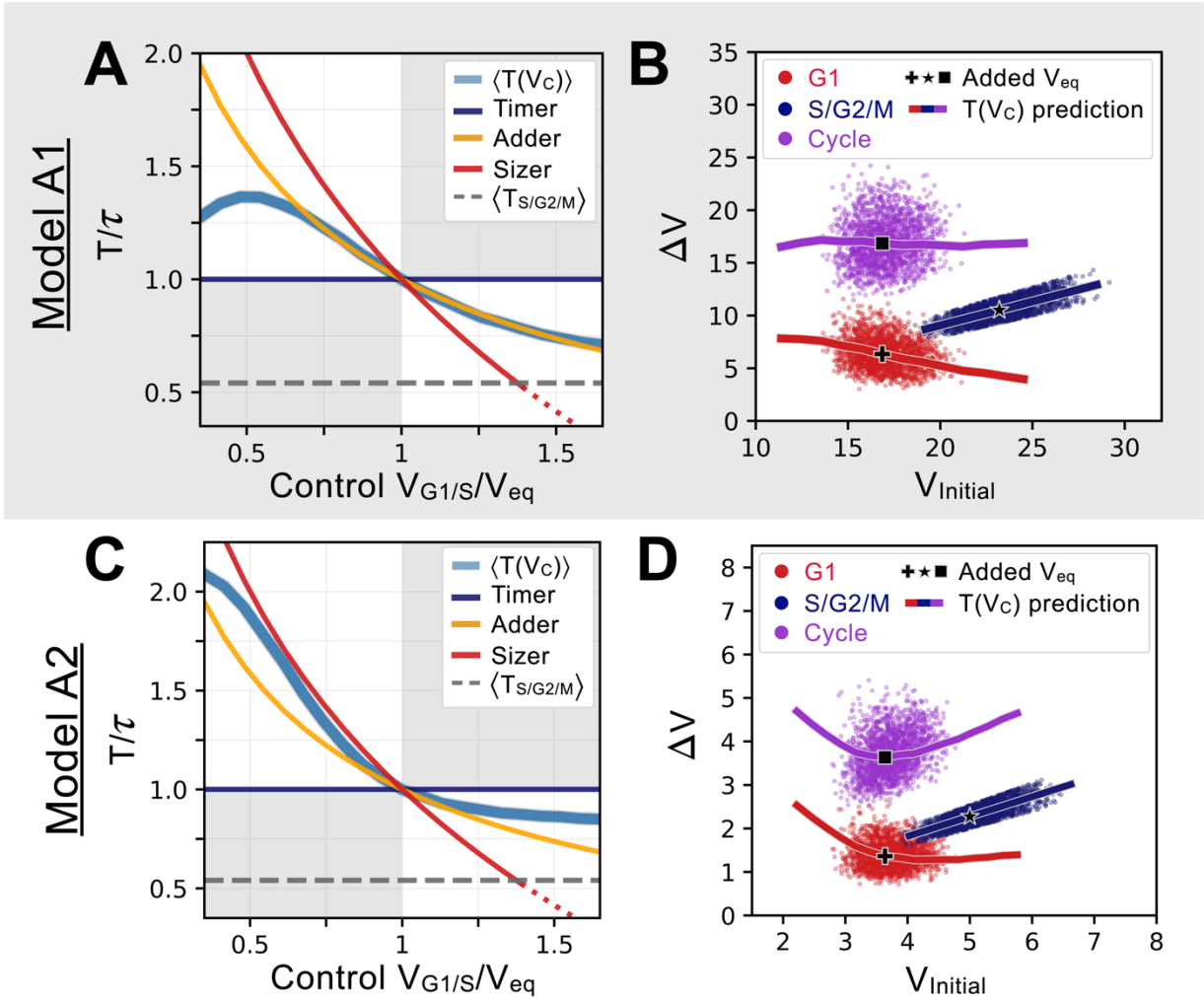

Figure 3 - Characterizing and comparing evolved size control mechanisms:
A) Average period $T(V_C)$ of the oscillator of Model A1 as a function of the control volume at the G1/S transition. Period is normalized by τ, the doubling time of the cell, and volume is rescaled by V_{eq}, the control volume such that $T(V_{eq}) = \tau$. Periods for the sizer (red), adder (orange) and timer (dark blue) are shown for comparison. Model A1 follows approximately the adder archetype over a large range of control volumes.
B) Added volumes ΔV for different phases of the cell cycles for simulations of Model A1. Individual dots correspond to different cell cycles. The full line corresponds to the extrapolation from the $T(V_C)$ curve shown in A. The black cross, star and square indicate the added volumes corresponding to when the system senses a volume corresponding to V_{eq} at the G1/S transition. We see that the model follows an adder over a large range of volumes.
C) Average period $T(V_C)$ of the oscillator of Model A2 with archetypes shown for comparison. We note that the $T(V_C)$ curve of this model is closer to the sizer at lower volumes and closer to a weak adder/timer at higher volumes relative to V_{eq}.

D) Added volumes ΔV for different phases of the cell cycles for simulations of Model A2, with similar conventions as panel B. Here we see the sizer behavior at lower volumes and the weak adder/timer behavior at higher volumes.

Figure 4

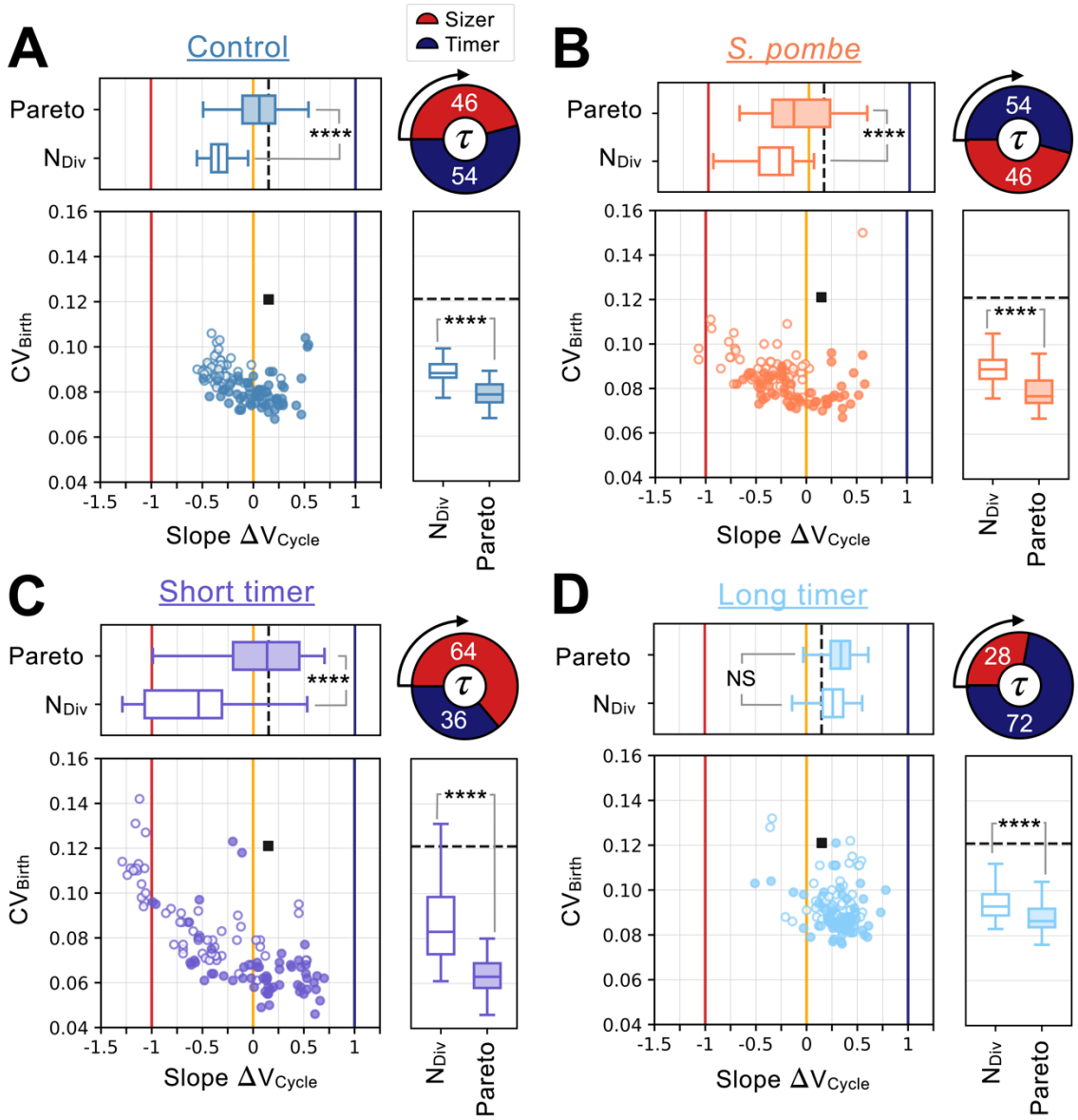

Figure 4 - Distinct network constraints and selection pressures bias size control evolution towards adders or sizers. Summary statistics for evolutionary simulations each having 500 epochs. Model A1 shown in Fig. 2 A) - G) was used as the initial seed network. 60 simulations were performed using Pareto optimization of the number of divisions (N_{Div}) and the CV of cell size at birth (CV_{Birth}), are labeled *Pareto* and are shown in full colors. 60 more simulations were performed using only the number of divisions as the fitness function, are labeled N_{Div} and are shown in colored outlines only. Scatter plots show the coefficient of variation of the size distribution at birth (CV_{Birth}, Y-coordinate) as a function of the fitted added volume slope over the whole cycle as a function of volume at birth (Slope ΔV_{Cycle}, X-coordinate) for the most fit models evolved during each of the 120 independent simulations. Horizontal box plots above the scatter plots display the distributions of the added volume slopes for the *Pareto* and N_{Div} simulations.

Timer (dark blue), adder (orange) and sizer (red) slopes are shown respectively at 1, 0, and -1 for comparison. Vertical box plots on the right of the scatter plots show the distributions of CV_{Birth} for the *Pareto* and N_{Div} simulations. Asterisks represent p-values for the Welch's t-Test between the distributions. The fitness value of N_{Div} and CV_{Birth} for the initial seed Model A1 are shown as a black square in the scatter plot or as a dashed black line in the box plots. Each panel explores different cell cycle structures which are summarized by the pie charts. Cycles begin on the left of the pie charts and rotate clockwise, indicating the order of the sizer (red) and timer (dark blue) phases. The labels indicate each phase's duration at equilibrium as a percentage of the doubling time τ.

A) Identical evolutionary parameters as for Model A1 evolution shown in Fig. 2A-G. G1 performs size control and has a duration 0.46τ at equilibrium and S/G2/M is a timer of duration 0.54τ. Welch's *t*-test $p < 10^{-4}$ for Slope ΔV_{Cycle}, $p < 10^{-4}$ for CV_{Birth}.

B) Evolution results for a cell cycle structure where the sizer and the timer phases of the cell cycle are inverted akin to *S. pombe*. G1 is a timer of duration 0.54τ and S/G2/M performs size control and has duration 0.46τ at equilibrium. Welch's *t*-test $p < 10^{-4}$ for Slope ΔV_{Cycle}, $p < 10^{-4}$ for CV_{Birth}.

C) Evolution results for a G1 size control of average duration 0.64τ at equilibrium where S/G2/M is a timer of duration 0.36τ. Welch's *t*-test $p < 10^{-4}$ for Slope ΔV_{Cycle}, $p < 10^{-4}$ for CV_{Birth}.

D) Evolution results for a G1 size control of average duration 0.28τ at equilibrium where S/G2/M is a timer of duration 0.72τ. Welch's *t*-test $p = 0.08$ for Slope ΔV_{Cycle}, $p < 10^{-4}$ for CV_{Birth}.

Figure 5

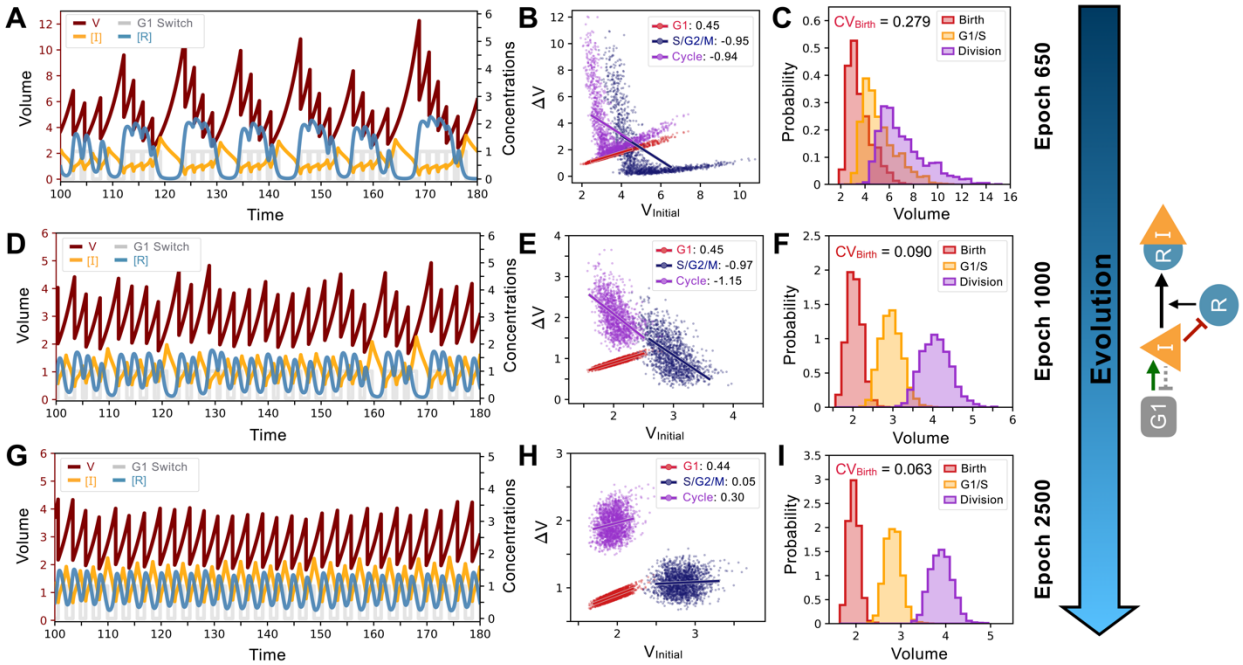

Figure 5 - System and evolutionary dynamics of cell size control networks.
Snapshots of an evolutionary simulation of 2500 epochs initialized with the Model A1 network topology along with an *S. pombe*-like cell cycle structure with a timer in G1 followed by a sizer in S/G2/M (see Fig. 4B). Pareto fitness optimization was performed using N_{Div} and CV_{Birth} as fitness functions. Rows indicate simulation results for the fittest networks from evolutionary epochs 650 (Panels A-C), 1000 (Panels D-F), and 2500 (Panels G-I). Network topology remains the same throughout the evolutionary simulation and is shown on the right.
A) Typical dynamics of the most fit model from epoch 650.
B) Added volumes ΔV for different phases of the cell cycle for the most fit model from epoch 650. Fitted slopes are indicated in the legend.
C) Size distributions at birth (red), G1/S (orange), and division (purple) for the most fit model from epoch 650. The coefficient of variation of the volume distribution at birth $CV_{Birth} = 0.279$.
D) Typical dynamics of the most fit model from epoch 1000.
E) Added volumes ΔV for different phases of the cell cycle for the most fit model from epoch 1000 Fitted slopes are indicated in the legend.
F) Size distributions at birth (red), G1/S (orange), and division (purple) for the most fit model from epoch 1000. The coefficient of variation of the volume distribution at birth $CV_{Birth} = 0.090$.
G) Typical dynamics of the most fit model from epoch 2500.
H) Added volumes ΔV for different phases of the cell cycle for the most fit model from epoch 2500. Fitted slopes are indicated in the legend.
I) Size distributions at birth (red), G1/S (orange), and division (purple) for the most fit model from epoch 2500. We see here that the sizer behavior from epoch 1000 was abandoned for a weaker adder overall yielding lower $CV_{Birth} = 0.063$.

Figure 6

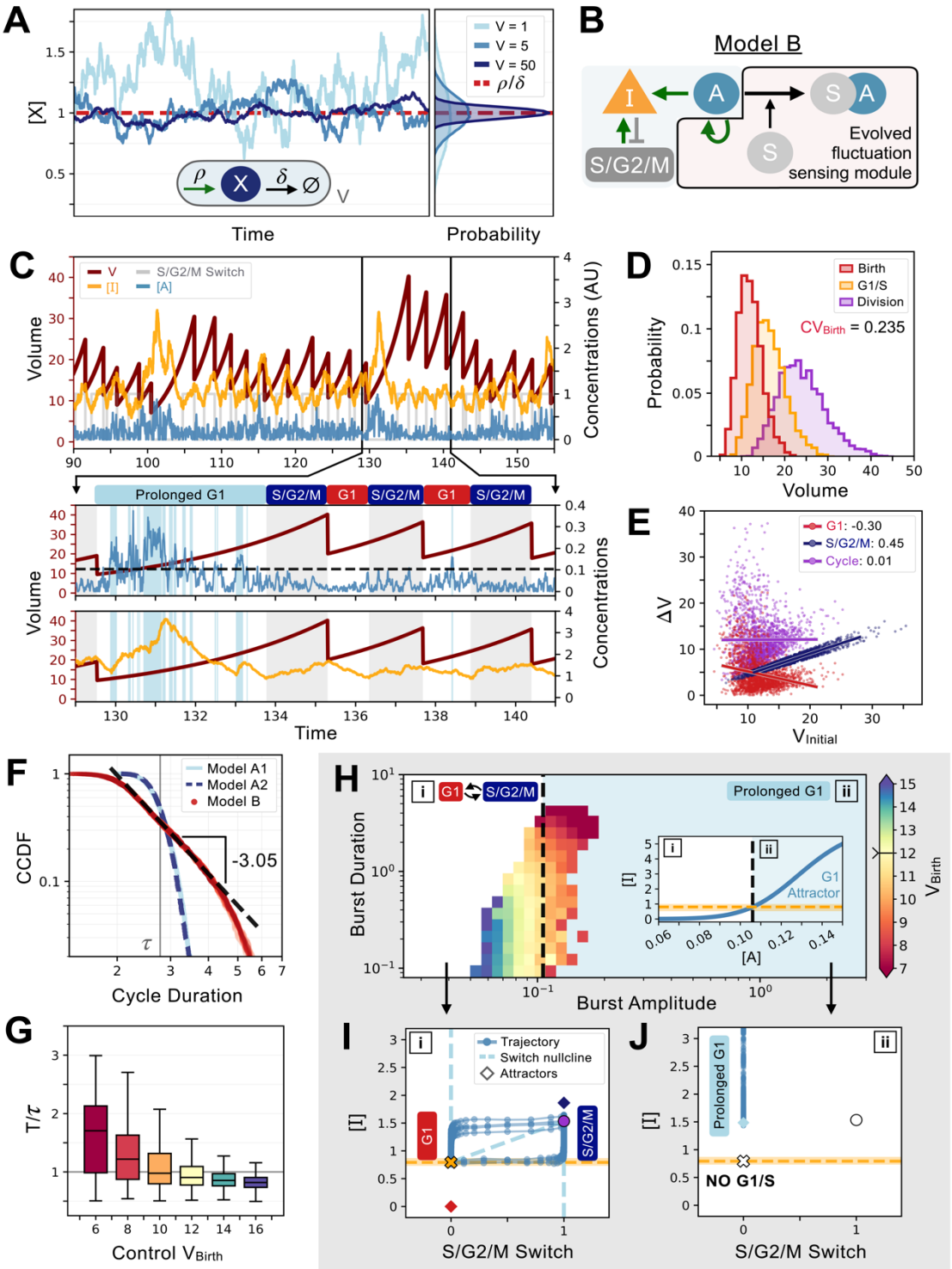

Figure 6 - An evolved concentration fluctuation sensing size control model exhibits self-organized criticality.

A) Size-dependent molecular noise arises due to Poissonian fluctuations in molecule number. Consider a protein production-degradation scheme for protein *quantity X* with production rate ρ

and degradation rate δ contained in a volume *V*. At equilibrium, the concentration of $[X]$ will be given by a distribution with mean ρ/δ and variance $\propto 1/V$. The effect of *V* on the molecular noise is shown on the time trajectories for simulations in a constant volume of *V* = 1 (light blue), *V* = 5 (medium blue), and *V* = 50 (dark blue). Corresponding concentration distributions are shown on the right-hand side of the panel.

B) Network topology of Model B which evolved to sense fluctuations. Here, the G1/S transition is controlled by the *concentration* of $[I]$ and not its *quantity*.

C) Characteristic cell cycle dynamics of Model B. Trajectories of $[I]$, $[A]$, and S/G2/M Switch are rescaled with arbitrary units (AU) for visualization purposes. Below, we zoom-in on 3 cycles to show how a low-volume induced burst in $[A]$ leads to a massive production of $[I]$ inducing a temporarily prolonged G1 phase. Subsequently, cells become bigger and display lower molecular noise inducing a comparatively shorter G1 phase.

D) Volume distributions at birth (red), G1/S (orange), and division (purple) for Model B. The coefficient of variation of the volume distribution at birth $CV_{Birth} = 0.235$.

E) Amount of volume added (ΔV) in G1 (red), S/G2/M (dark blue), and over the whole cycle (purple) as a function of their initial volume at the beginning of these phases, *i.e.,* birth for G1 and cycle, and G1/S for S/G2/M, with the slope of linear fits indicated in legend.

F) Complementary cumulative distribution functions of the cycle duration (CCDF; probability that the cell cycle duration is larger than the value on the X-axis) for three models discussed in the main text: Model A1 (light blue), Model A2 (dashed dark blue), and Model B (red). The light grey line indicates the doubling time τ. We see that Model B exhibits a long tail past the doubling time, which is consistent with a power-law scaling of the cycle duration probability. We find a criticality indicative scaling exponent of -3.05 for the CCDF after fitting the tail of the distributions of 5 independent realizations of the dynamics of Model B.

G) Box plots of the cycle length distributions as a function of control volume V_C at birth. Cycle lengths are normalized by the doubling time τ. Here, V_C sets the molecular noise level to be equivalent to that of an exponentially growing cell born at V_C but whose volume is reset to V_C at each division. Note the very long tail of the distributions at small V_C.

H) Activator protein $[A]$ is synthesized in bursts whose amplitude and duration are a function of volume. We define the burst duration as the total time during which $[A]>0$ for a cycle. The burst amplitude corresponds to the average level of $[A]$ during each G1 phase. Each burst is then color-coded as a function of the birth volume of the cell that induced it. We use a divergent colormap whose center value (light yellow) corresponds to the average volume of the cells at birth and is indicated by a notch on the colorbar. The black dashed line corresponds to the level of $[A]$ which triggers a transition between two modes of growth and division as shown in the inset by the position of the G1 attractor for $[I]$ becoming equal to the concentration required to induce the G1/S transition. Here, (i) corresponds to the deterministic regime when volume is high and (ii) corresponds to the noisy regime when volume is low. Note that the average volume of the cells at birth is positioned close to the black dashed line.

I) Phase-space representation of the relaxation oscillator in the deterministic regime (i). The X-coordinate shows the S/G2/M Switch variable, and the Y-coordinate shows the concentration of $[I]$. Here, when volume is high, the position of the G1 attractor is *below* the $[I]$ concentration at which the G1/S transition happens. Thus, G1/S takes place and cells are in the cell cycle with a period of ~0.85τ.

J) Phase-space representation of the noisy regime (ii). Here, when volume is low, the position of the G1 attractor becomes *greater* than the $[I]$ concentration at which the G1/S transition happens, and cells remain temporarily stuck in a prolonged G1 state and are unable to trigger the G1/S transition.

Supplementary materials

In Section 1, we first describe how to modify deterministic and stochastic ODEs to account for a exponentially growing cell volume. In Section 2, we describe the 3 size control archetypes, namely the timer, the adder, and the sizer, as well as our implementation of the initial seed cell cycle model. Then, in Section 3, we give details on the φ-evo evolutionary algorithm. Finally, in Section 4 we provide parameter values and equations for the models presented in the main text as well as for additional models produced by our evolutionary simulations.

1. MATHEMATICAL IMPLEMENTATION

A. Deterministic

All biochemical concentrations can be described as a quantity of molecules of a biochemical species divided by the volume that contains it. The fundamental equation describing all concentrations is thus:

$$[X](t) = \frac{X(t)}{V(t)} \tag{S1}$$

Here, $X(t)$ is the quantity of molecules of an arbitrary biochemical species X as a function of time and $V(t)$ is the volume of the cell containing said species as a function of time. We will use the bracket notation $[X](t)$ for concentrations. In this project, we will model all biochemical species directly at the concentration level and assume proteins are uniformly distributed in an exponentially growing cell volume. The absolute growth rate of the cell λ is chosen to be constant over a large viable range of cell volume and is otherwise 0. Consequently, volume grows over time with a fixed absolute growth rate $\lambda = 0.25$ over a viable volume range following the equation:

$$\frac{dV}{dt} = \lambda V(t) \tag{S2}$$

Deterministic rate equations describing the dynamics of the biochemical species at the concentration level have to be adjusted to take into consideration a time-varying volume. From equation S1 and the derivative chain rule, we get:

$$\frac{d[X]}{dt} = \frac{d}{dt}\frac{X(t)}{V(t)} = \frac{1}{V(t)}\frac{dX}{dt} - \frac{X(t)}{V(t)^2}\frac{dV}{dt}$$

which we can combine with equation S2 to give:

$$\frac{d[X]}{dt} = \frac{1}{V(t)}\left(\frac{dX}{dt}\bigg|_{V=\text{Cst}}\right) - \lambda[X](t) = f([X](t)) - \lambda[X](t) \tag{S3}$$

The first term in the equation S3, $f([X](t))$, corresponds to the usual biochemical reaction rates that occur when the volume of the cell is fixed. The second term, $-\lambda[X](t)$, is a dilution term that we can interpret as an effective degradation of the concentration $[X](t)$ due to the exponential growth of the cell volume over time.

To further simplify the expression for $f([X](t))$, we make an assumption about the production rates of all biochemical species in our models. Let us consider the rate equation describing the dynamics of the quantity of an arbitrary protein X with generic production rate ρ and degradation rate δ contained in a fixed cell volume V.

$$\frac{dX(t)}{dt} = \rho - \delta X(t)$$

Here, $f([X](t))$ is given by:

$$f([X](t)) = \frac{1}{V}\frac{dX(t)}{dt} = \frac{\rho}{V} - \delta[X](t)$$

We assume that all the proteins in our models are constitutively expressed by the cell. In other words, the production rates ρ are linear functions of the cell volume $\rho = \rho(V(t)) = \rho_0 V(t)$. This ensures that the protein production rates scale with the volume such that concentrations stay constant over time which is a general feature of most proteins in *S. cerevisiae* [1–3]. This yields:

$$f([X](t)) = \rho_0 - \delta[X](t)$$

Taken altogether with equation S3, the deterministic dynamics of a constitutively expressed arbitrary protein concentration $[X](t)$ contained in an exponentially growing cell volume are given by:

$$\frac{d[X]}{dt} = \rho_0 - (\delta + \lambda)[X](t) \tag{S4}$$

B. Stochastic

To simulate molecular noise, we follow a classical tau-leaping formalism [4]. Specifically, we choose the Euler-Maruyama implementation to generate approximate solutions to stochastic differential equations [5].

As we have done before in the deterministic case, let us first consider the quantity of an arbitrary protein $X(t)$ in order to extract the equation for the concentration $[X](t)$. Let's assume $X(t)$ is changing via a *single* biochemical reaction rate $\frac{dX}{dt} = g(X(t))$ over the time interval $[0, T]$ given $X(t = 0) = X_0$. We will show later how this approach can be generalized to include multiple reaction rates. We begin by partitioning the time interval in N equal segments of length Δt such that $0 < t_1 < t_2 < ... < t_N = T$ with $t_n = n \cdot \Delta t$, $n \in \{1, N\}$.

The Euler-Murayama approximate solution to the stochastic differential equation at the discrete time points t_n is then recursively given by the following equation for $n \in \{1, N-1\}$ where the single biochemical reaction is assumed to happen with a Poisson rate (corresponding to the deterministic rate), which adds one white Gaussian noise to the differential equations with a variance equal to that rate:

$$X_{n+1} = X_n + g(X_n)\Delta t + \sqrt{|g(X_n)|\Delta t} \cdot \mathcal{N}(0,1) \tag{S5}$$

Here, $X_n = X(t_n)$, $g(X_n)$ is the drift term, $\sqrt{|g(X_n)|}$ is the diffusion term and $\mathcal{N}(0,1)$ is a random Gaussian variable of mean 0 and variance 1. In other words, X_{n+1} is a random Gaussian variable of mean $X_n + g(X_n)\Delta t$ and variance $|g(X_n)|\Delta t$. Since this describes the quantity of proteins, we also have to consider the change in

volume over time to recover the equation for the concentration of proteins, $[X](t)$. Thus, let's consider the volume of the cell $V(t)$ at the discrete time points t_n, which is given recursively by the equation:

$$V_{n+1} = V_n + \lambda V_n \Delta t = V_n(1 + \lambda \Delta t) \tag{S6}$$

Here, we define $V_n = V(t_n)$ and recover the λV_n term from equation S2. We assume that the volume time evolution is noiseless for simplicity. To recover, the differential equation describing the protein concentration, we evaluate the expression $[X]_{n+1} = \frac{X_{n+1}}{V_{n+1}}$. Thus, combining equations S5 and S6, we get:

$$[X]_{n+1} = \frac{X_n + g(X_n)\Delta t + \sqrt{|g(X_n)|\Delta t} \cdot \mathcal{N}(0,1)}{V_n(1 + \lambda \Delta t)}$$

$$[X]_{n+1} = \frac{1}{1 + \lambda \Delta t}\left([X]_n + g([X]_n)\Delta t + \sqrt{\frac{|g([X]_n)|\Delta t}{V_n}} \cdot \mathcal{N}(0,1)\right)$$

Where we identify $\frac{1}{V_n} g(X_n) = g([X]_n)$ as the rate equation describing the *concentration* of the consitutively expressed protein $[X](t)$ when the volume V is fixed as described in the deterministic case. Then, we compute the derivative as:

$$\begin{aligned}
\left.\frac{d[X]}{dt}\right|_{t_n} &\approx \frac{[X]_{n+1} - [X]_n}{\Delta t} \\
&= \frac{1}{\Delta t(1 + \lambda \Delta t)}\left([X]_n - (1 + \lambda \Delta t)[X]_n + g([X]_n)\Delta t + \sqrt{\frac{|g([X]_n)|\Delta t}{V_n}} \cdot \mathcal{N}(0,1)\right) \\
&= \frac{1}{1 + \lambda \Delta t}\left(g([X]_n) - \lambda [X]_n + \sqrt{\frac{|g([X]_n)|}{V_n \Delta t}} \cdot \mathcal{N}(0,1)\right)
\end{aligned}$$

Finally, we recover the approximate full differential equation for the protein concentration by expanding the prefactor in the last equation to the 0th order in Δt assuming it to be small to give:

$$\left.\frac{d[X]}{dt}\right|_{t_n} \approx g([X]_n) - \lambda [X]_n + \sqrt{\frac{|g([X]_n)|}{V_n \Delta t}} \cdot \mathcal{N}(0,1) \tag{S7}$$

So far, we have assumed that there is only a *single* biochemical reaction rate $g([X](t))$. We can however easily generalize our approach to include additional reaction rates by summing up the contribution of each rate to the total differential equation. Given M independent reaction rates $g_i([X](t))$ and the properties of random Gaussian variables, we can easily generalize:

$$\left.\frac{d[X]}{dt}\right|_{t_n} \approx \sum_{i=1}^{M} g_i([X]_n) - \lambda [X]_n + \sum_{i=1}^{M}\left(\sqrt{\frac{|g_i([X]_n)|}{V_n \Delta t}} \cdot \mathcal{N}_i(0,1)\right) \tag{S8}$$

Importantly, the $\mathcal{N}_i$ are Gaussian vectors accounting for the noise correlations associated with single reactions. For instance, imagine one protein X_k turns into

another protein X_p, then the corresponding Gaussian vector for this interaction takes the form $\mathcal{N}(0,1)(\vec{x_k} - \vec{x_p})$ where $\vec{x_k}$ is vector of length corresponding with the number of variables in the system whose k-th component is equal to 1 with 0s elsewhere. This indicates that the molecular fluctuation due to this reaction should have opposite signs for X_k and X_p as expected.

The term $\lambda[X]_n$ is a dilution term that corresponds to an effective degradation of protein concentration $[X]_n$ as seen in the deterministic case. Interestingly, we highlight the $\frac{1}{V_n}$ dependency in the noise term. We can understand this dependency intuitively by considering a protein production process with a Poisson parameter θ. In this scenario, the mean and the variance of the protein quantity distribution is given by the parameter θ. Going back to concentration space, there are an infinite number of combinations of protein quantity and volume that can give the same concentration $[X] = X/V$. Thus, we need to specify both the protein number X and the volume V to correctly model the molecular noise contributing to fluctuations in concentrations.

2. SIZE CONTROL

A. Initial seed network

To guide the evolutionary process, we begin with an initial seed network. We base our first seed network on the phenomenology of the budding yeast *S. cerevisiae*'s cell cycle, where cell size primarily regulates the timing of the START transition in late G1 [6]. This regulation allows small daughter cells to delay the G1/S transition allowing them to catch-up in size by extending the G1 phase. S/G2/M duration on the other hand is largely independent of cell size. We note that while budding yeast divide asymmetrically, our simulated cells divide symmetrically. In our simple initial seed network, the cell cycle consists of two phases, G1 and S/G2/M, which respectively denote the pre-G1/S and post-G1/S phases of the cell cycle. The transition between these two phases is controlled by the level of a transcription regulator we call **I**. Like the Whi5 protein in *S. cerevisiae*, **I** is an inhibitor of the G1/S transition such that the lower its level, the higher the chances of cell cycle progression. Since protein production rates were assumed to be dependent on volume (as described in Section 1), we found that **I**'s concentration alone was largely independent of volume and could not trigger a size-dependent G1/S transition as Whi5 does in budding yeast. Thus, we chose the quantity of **I** defined as $\mathbf{I}(t) = [\mathbf{I}](t) \times V(t)$ as the control variable for this transition. We chose to model the probability of the G1/S transition occurring at the next time point of the simulation with a sigmoid-shaped curve given by equation S9 that can be visualized in **Fig.S1**. We maintain $\theta = 0.8$ and $n_\theta = 8$ fixed throughout this project.

$$\mathcal{P}_{\mathrm{G1/S}}(t) = \frac{2}{1 + \exp\left((\mathbf{I}(t)/\theta)^{n_\theta}\right)} \tag{S9}$$

In our seed model, we encode cell cycle state using a binary variable **S/G2/M Switch**, which is 0 in G1 and turns to 1 in S/G2/M once the G1/S transition takes place. Following *S. cerevisiae*'s cell cycle structure where S/G2/M duration is independent of cell size, we fix S/G2/M duration to be $\sim 50\%$ of the doubling time $\tau = \frac{1}{\lambda} \ln 2$ with uniform noise unless stated otherwise. This way, cells can tune the length of their cell cycle by adjusting G1 length while being constrained by the

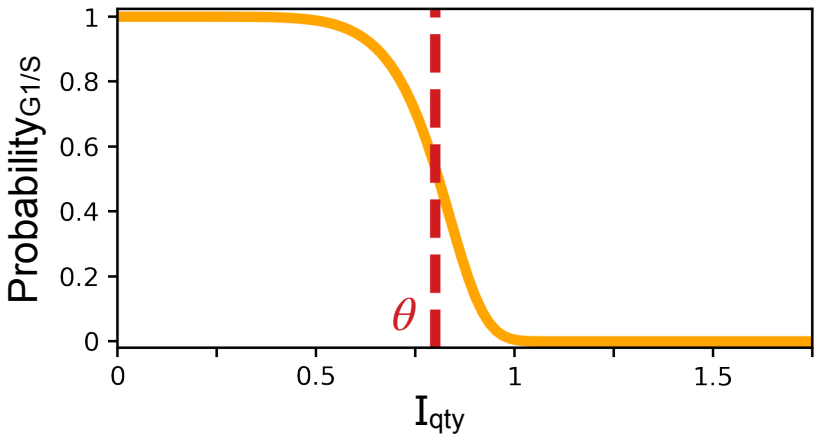

Fig. S1. Probability of the G1/S transition occurring at the next time step. X-coordinate is the quantity of the transcriptional regulator **I**. Y-coordinate is the probability of the G1/S transition occurring at the next time step Δt. Parameters $\theta = 0.8$ and $n_\theta = 8$.

incompressible length of the timer in S/G2/M, $T_{\text{S/G2/M}}$.

Following S/G2/M, cells divide symmetrically such that $V_{\text{Birth}}^{(n+1)} = V_{\text{Division}}^{(n)}/2$. The n exponent here is referencing the n-th generation in the cell lineage. We assume perfect partitioning of all proteins between the two daughter cells such that the proteins' concentrations remain the same before and after division. After division, we follow one of the two daughter cells during their own subsequent cycle. If we simulate the cell lineage for a long time, ergodicity guarantees that all volume states will be visited given stable growth and we can extract population statistics from the lineage data itself.

Inspired by the dynamics of Whi5, which is produced in S/G2/M and diluted in G1, we chose an initial seed network where **S/G2/M Switch** activates the transcription of the **I** inhibitor. This ensures that the concentration $[\mathbf{I}]$ is "reset" to a higher value following S/G2/M and prevents cells from skipping entirely the G1 phase of the subsequent cycle which would quickly send the volume of the cell converging quickly towards 0. We note that this interaction systematically appeared anyway in our early evolution simulation so we chose to include it in the initial seed network to accelerate the evolutionary process.

B. Size control archetypes

Size control mechanisms are often compared to 3 well characterized models or archetypes in order to quantify the strength of the size control mechanism under study. Specifically, there are **timers**, **adders** and **sizers**. In this subsection, we will define each archetype and show that we can summarize them via a control volume response curve $T(V_C)$ as described in the main text.

First, let's consider the timescale of growth. Given $V(t = 0) = V_0$, the solution $V(t)$ of the volume equation S2 is $V(t) = V_0 e^{\lambda t}$. From this equation we can easily recover the doubling time τ defined as the time required to double a cell's volume

$(V(\tau) = 2V_0)$ which yields:

$$\tau = \frac{1}{\lambda} \ln 2 \tag{S10}$$

The doubling time τ is only a function of the growth rate λ. Since we are only considering symmetrical division events, fixed interdivision times shorter than the doubling time will yield progressively smaller daughter cells. Similarly, fixed interdivision times longer than the doubling time will yield progressively larger daughter cells. Thus, the absolute growth rate λ sets the timescale for cell cycle dynamics if we want to simulate a stable cell lineage.

With the quantity sensing of the inhibitor **I** at the G1/S transition (see equation S9), we find that the instantaneous volume at G1/S sets the concentration of the biochemical species for the rest of the cycle and until the next G1/S transition in the daughter's cell cycle. Consequently, it regulates the timing of the G1 phase of the daughter cell and thus creates a return map for the volume at G1/S. We find that the volume at G1/S at the $(n+1)$-th generation $V_{\mathrm{G1/S}}^{(n+1)}$ is given recursively by:

$$V_{\mathrm{G1/S}}^{(n+1)} = \frac{V_{\mathrm{G1/S}}^{(n)} \cdot e^{\lambda(T_{\mathrm{S/G2/M}} + T_{\mathrm{G1}}(V_{\mathrm{G1/S}}^{(n)}))}}{2} = \frac{V_{\mathrm{G1/S}}^{(n)} \cdot e^{\lambda T(V_{\mathrm{G1/S}}^{(n)})}}{2}$$

To study the mechanisms of cell size control, we choose to define a useful new variable: the control volume V_C. This control variable is independent from the biochemical network and maintained fixed allowing us to break the size feedback, and distinguish its input, the volume V, from its output, the induced cycle period T. With this new variable, we can modify the control at G1/S by forcing the transitions to trigger once $I_C = [I] \times V_C$ is low enough. We can then extract the response curve of the system, *i.e.* the cell cycle period induced from sensing this control volume at G1/S $T(V_C)$. We represent this process schematically in **Fig.S2-A**.

The control volume at which the response curve $T(V_C)$ is equal to the doubling time τ corresponds to the **equilibrium volume**, V_{eq}, for this network. Indeed, if $T(V_{\mathrm{eq}}) = \tau$, then the cell cycle length will ensure that this cell exactly doubles its volume during its cell cycle and returns to the same V_{eq} at the next generation. This volume is a fixed point of the volume return map and can be either stable or unstable. Theoretically, there could be size control mechanisms with multiple fixed points of the response curve, but practically we have not seen this emerge from any of our evolution experiments and therefore assume that V_{eq} is unique.

Size variation naturally occurs in our models due to the precise timing of G1 and S/G2/M cycle phases which are both noisy, so the volume does not stay at V_{eq} for very long. The stability of growth around this equilibrium volume however will depend on the sign of the local derivative with respect to control volume of the $T(V_C)$ response curve and we will consider the following 3 cases:

- $T(V_C)$ is strictly <u>increasing</u> with V_C. In this case, small deviations around V_{eq} are amplified over successive generations and the volume quickly shrinks to 0 or explodes to ∞. In this case, we say that V_{eq} is an unstable fixed point of the response curve.

- $T(V_C)$ is <u>constant</u> with V_C. In this special case and assuming exponential growth of the volume, the only stable mode of growth corresponds to the response curve $T(V_C) = \tau$. This corresponds to the only stable timer archetype.

In this particular scenario, V_{eq} is not well defined as there are an infinite number of volumes where the response curve intersects the doubling time.

- $T(V_C)$ is strictly decreasing with V_C. In this case, cells correct for size deviations over successive generations and perform size control. In this case, we say that V_{eq} is a stable fixed point of the response curve.

Here, we found the $T(V_C)$ curves that were selected by the evolutionary algorithm were all decreasing with V_C as expected for stable size control mechanisms. Thus, for the remainder of this document, we will assume that V_{eq} is uniquely defined and corresponds to a stable fixed point of the control volume response curve.

B.1. Timer

The **timer** archetype describes mechanisms that monitor time rather than size. If the cycle duration of the timer is tuned precisely to the doubling time $\tau = \frac{1}{\lambda}\ln 2$, cells will double their mass over the course the cell cycle to ensure that newborn daughter cells have the same volume at birth as their mothers did when they were born. Consequently, this category of mechanisms is notoriously bad at correcting for size deviations given exponential cell volume. If growth was linear however, this mechanism would allow for size control to take place.

$$T_{\text{Timer}}(V_C) = \tau = \frac{1}{\lambda}\ln 2 \tag{S11}$$

B.2. Adder

The **adder** archetype describes mechanisms where cells add a constant amount of cell volume during each cycle. We define Δ the increment of added volume between birth and division, that is $\Delta = V_{\text{Division}} - V_{\text{Birth}}$. For adder mechanisms, the added volume at each cycle is constant and does not depend on cell size. In this case, initial size deviations are reduced by a factor of 2 at each division such that the volume at birth geometrically converges to the added volume Δ over successive generations. To recover the adder response curve $T_{\text{Adder}}(V_C)$, we consider that by definition, $V^{\text{Division}} = V^{\text{Birth}} e^{\lambda T_{\text{Adder}}}$. From this equation and the definition of the adder, we can recover the cycle period T_{Adder}:

$$T_{\text{Adder}}(V_{\text{Birth}}) = \frac{1}{\lambda}\ln\left(\frac{\Delta}{V^{\text{Birth}}} + 1\right)$$

We would like write this equation as a function of the control volume V_C at G1/S and the equilibrium volume V_{eq} alone. Assuming that the G1/S transition is followed by a timer in S/G2/M, we can write $V_{\text{Birth}} = V_C e^{\lambda T_{\text{S/G2/M}}}/2$. Similarly, since we know by definition that $T_{\text{Adder}}(V_{\text{eq}}) = \tau$, we can recover that the added volume increment is $\Delta = V_{\text{eq}} e^{\lambda T_{\text{S/G2/M}}}/2$. Finally, we can combine these two expressions with to recover the final expression of the adder response curve:

$$T_{\text{Adder}}(V_C) = \frac{1}{\lambda}\ln\left(\frac{V_{\text{eq}}}{V_C} + 1\right) \tag{S12}$$

We note here that if the control volume was measured at division or at birth, the response curve of the adder would be unchanged. The only difference would be that both V_C and V_{eq} would correspond to volumes at division or birth volumes

instead of volume at the G1/S transition. Here for example, the volume increment Δ corresponds to the V_{eq} at birth.

B.3. Sizer

The **sizer** archetype describes mechanisms that measure size directly and allow a cell to return to a target volume V_{Target} after a single generation, irrespective of how big or small a cell was initially. For sizers, $V^{\text{Division}} = V_{\text{Target}} = V^{\text{Birth}} e^{\lambda T_{\text{Sizer}}}$ by definition.

We can then extract:

$$T_{\text{Sizer}}(V_{\text{Birth}}) = \frac{1}{\lambda} \ln \left(\frac{V_{\text{Target}}}{V_{\text{Birth}}} \right)$$

We can then write V_{Birth} and V_{target} as a function of the control volume at G1/S V_C and the equilibrium volume V_{eq}. Using the same definitions as before $V_{\text{Birth}} = V_C e^{\lambda T_{\text{S/G2/M}}}/2$ and $T_{\text{Sizer}}(V_{\text{eq}}) = \tau$, we find that $V_{\text{target}} = V_{\text{eq}} e^{\lambda T_{\text{S/G2/M}}}$. The sizer response curve thus follows:

$$T_{\text{Sizer}}(V_C) = \frac{1}{\lambda} \ln \left(\frac{2V_{\text{eq}}}{V_C} \right) \tag{S13}$$

We note again here that if the volume was measured at division or at birth, the equation for the sizer would be identical with the only difference being that the control volume V_C and the equilibrium volumes V_{eq} would correspond to division or birth volumes respectively.

The three archetypes' response curves are shown in **Fig.S2**. From these curves and given the particular cell cycle structures we examined, we can extract multiple relevant measures of size control such as the volume at birth, G1/S, and division from which we get the added volume during each phase of the cell cycle. It is noteworthy that the derivative of the added volumes ΔV with respect to the birth volume V^{Birth} for the timers, adders, and sizers, are respectively 1, 0, and -1. Size control mechanisms are typically compared to the 3 archetypes by measuring the amount of added cell volumes over their cell cycles ΔV_{Cycle} and then fitting a linear model to these data points. The fitted slope of the linear model then informs what archetype this particular mechanism is more akin to. Some models evolved with added volume slopes lower than -1 and we call those **super-sizers**. Such mechanisms overcompensate for volume deviations about the equilibrium value which can increase variation in the size distribution instead of decreasing it.

C. Response curve of the seed networks

In light of the control volume and response curve definitions from subsection B, we can revisit the initial seed model and investigate how different assumptions alter the stability of growth and division in a cell lineage. Specifically, we investigate the size scaling assumption of the protein production rates and the concentration vs. quantity sensing of the transcriptional regulator **I** at G1/S as previously described in Section 1. We summarize our results in **Fig.S3**.

First, let us consider the G1 trajectory of the transcriptional regulator $[\mathbf{I}]$ who is solely produced during the S/G2/M timer. The dynamics of $[\mathbf{I}](t)$ in G1 will be described by the following equation:

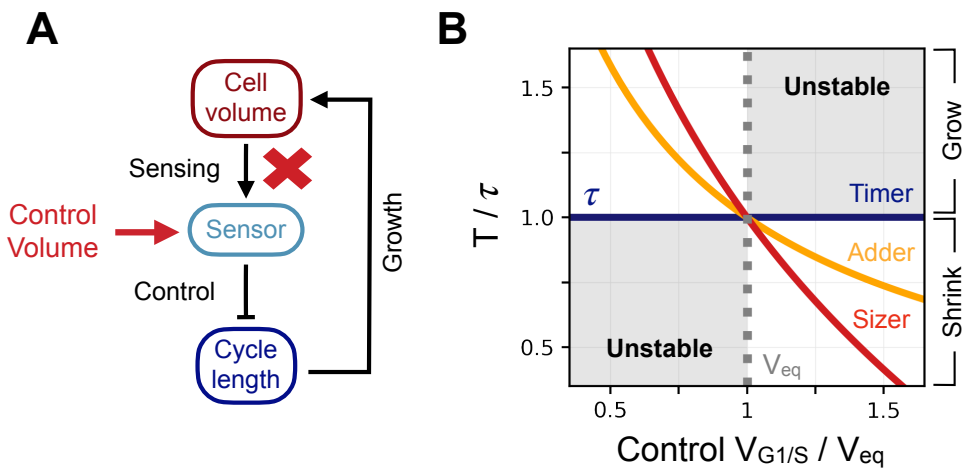

Fig. S2. Control volume and archetype response curves.
A - Schematic representation of the way we break the feedback in the system and impose a control volume V_C (red arrow) at the G1/S transition in order to record the induced cell cycle period $T(V_C)$. **B** - Response curve of the 3 size control archetypes. X-coordinate is the control volume at G1/S V_C normalized by the equilibrium volume V_{eq}. Y-coordinate is the response curve of the models $T(V_C)$ normalized by the doubling time τ. The dark blue curve is the response curve for the timer of length τ, the orange curve the response curve for the adder, and the red curve the response curve for the sizer. The dotted grey line indicates the equilibrium volume V_{eq}. The shaded region corresponds to the region where growth is unstable and volume diverges over successive generations.

$$[\mathbf{I}](t) = [\mathbf{I}]_0 e^{-(\delta+\lambda)t} \tag{S14}$$

Here, the time variable t represents the time since birth, $[\mathbf{I}]_0 = [\mathbf{I}](t=0)$, δ is the protein's degradation rate and λ is the growth rate of the cell volume. This equation holds until the G1/S transition where the S/G2/M Switch is turned on again and G1 ends. Because the degradation of the inhibitor does not yet depend on volume in any way, the time spent in G1 will only be dependent on the ratio between: 1) the initial condition at birth $[\mathbf{I}]_0$; 2) the final condition at the G1/S transition, $[\mathbf{I}]_{\text{G1/S}}$.

We found that the size scaling assumption of the protein production rates influences the initial condition at birth $[\mathbf{I}]_0$. When production rates scale with size, we find that $[\mathbf{I}]_0$ is independent of volume. This is expected as this assumption was chosen specifically to model proteins whose concentrations are independent of size. Conversely, when we modify this assumption and consider that protein production rates are independent of size (e.g. like Whi5 in budding yeast), we find that the system produces a constant quantity of inhibitor instead of a constant concentration. This means that the initial concentration at birth $[\mathbf{I}]_0$ scales as $1/V$.

Similarly, when imposing quantity sensing of **I** at G1/S, we found that the concentration of inhibitor at G1/S $[\mathbf{I}]_{\text{G1/S}}$ scales as $1/V$. Finally, when imposing concentration sensing of **I** at G1/S, we found a constant concentration of inhibitor at G1/S $[\mathbf{I}]_{\text{G1/S}}$ as was expected by design.

Together, those assumptions alter the scaling of the duration of the G1 phase

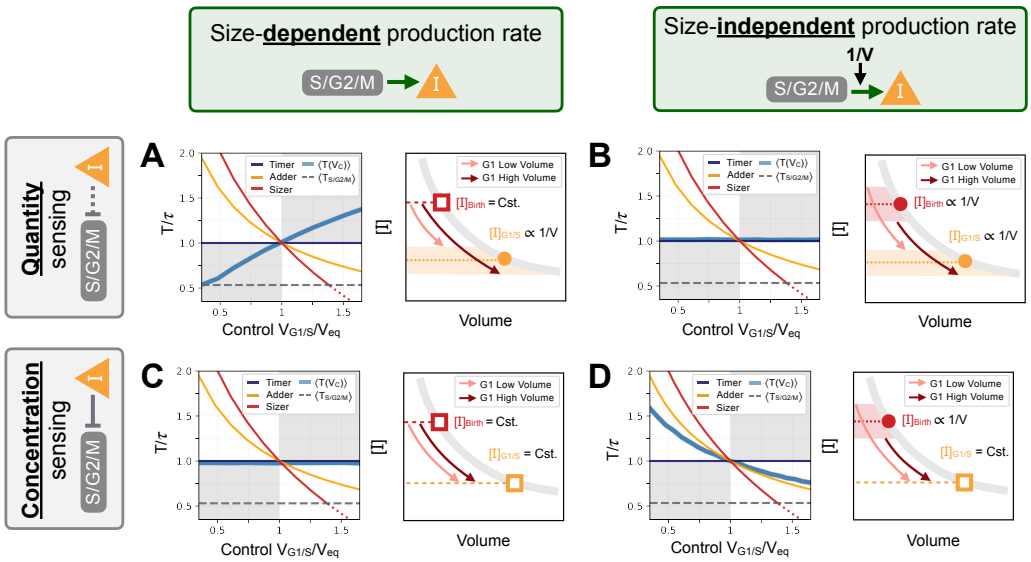

Fig. S3. Response curves for the initial seed networks
Columns indicate the size scaling assumption of the protein production rates as indicated above the figure. Rows indicate quantity or concentration sensing of inhibitor **I** at the G1/S transition assumption as indicated on the left side of the figure. In each panel, we first show the seed network's response curve $T(V_C)$ as a function of control volume V_C at G1/S. Sizer (red), adder (orange) and timer (dark blue) archetypes are shown for comparison. Second, we provide a schematic representation of the $[\mathbf{I}]$ trajectory in G1. Schematic trajectories are shown for low volumes (light pink) and high volumes (dark red). **A** - Quantity sensing of **I** at G1/S with a size-dependent production rate in S/G2/M. Here, cells are born with a constant concentration $[\mathbf{I}]$. Because of the quantity sensing at G1/S, the concentration of $[\mathbf{I}]$ at G1/S scales as $1/V$. Thus, the time spent in G1 scales with V. This is the initial seed network we chose for most of our evolution experiments. **B** - Quantity sensing of **I** at G1/S with a size-independent production rate in S/G2/M. Here, cells are born with a concentration $[\mathbf{I}]$ at birth that scales as $1/V$. Because of the quantity sensing at G1/S, we again find that the concentration of $[\mathbf{I}]$ at G1/S scales as $1/V$. Thus, the time spent in G1 is constant. **C** - Concentration sensing of $[\mathbf{I}]$ at G1/S with a size-dependent production rate in S/G2/M. Here, cells are born with a constant concentration $[\mathbf{I}]$. Because of the concentration sensing at G1/S, we find that the concentration of $[\mathbf{I}]$ at G1/S is constant. Thus, the time spent in G1 is constant. **D** - Concentration sensing of $[\mathbf{I}]$ at G1/S with a size-independent production rate in S/G2/M. Here, cells are born with a concentration $[\mathbf{I}]$ that scales as $1/V$. Because of the concentration sensing at G1/S, we find that the concentration of $[\mathbf{I}]$ at G1/S is constant. Thus, the time spent in G1 scales as $1/V$.

of the initial seed cycle. We summarize these results and present the models' response curves $T(V_C)$ in **Fig.S3** where each row and column corresponds to a specific combination of assumptions. There, in **A**, we see that for the combination of size-scaling production rate and quantity sensing at G1/S, we get a cell cycle period that is increasing with control volume V_C. This is undesirable and leads to unstable

growth of the cell lineage towards 0 or ∞, but rewards the evolution of size control mechanisms that can prevent this unstable growth. We chose this initial seed model for most of our evolutionary simulations. In **B** and **C**, we found that the two assumptions compensated each other to create size-independent timer models. The parameters of the network can be precisely fine-tuned to yield a response period of exactly τ as was done to produce the response curves shown here. Thus, it is technically possible to evolve a size control mechanism using these initial seed models, but we chose not to go down that path because we wanted to evolve an active size control mechanism. Finally, in **D**, we see that if we assume that protein production rates do not scale with size and that the G1/S transition depends on the concentration of inhibitor $[\mathbf{I}]$, we get an initial seed model that already accomplishes size control as it displays a response curve that decreases with control volume V_C. This simple model loosely corresponds to the Whi5 inhibitor dilution model of budding yeast [6] where a constant quantity of inhibitor Whi5 is present at birth (and thus a concentration $[\text{Whi5}] \propto 1/V$) and is passively diluted in G1 until it reaches concentration threshold that triggers the G1/S transition.

3. EVOLUTIONARY ALGORITHM

Here we briefly describe the φ-evo evolutionary algorithm from [7] that we used to evolve size control networks. We refer the reader to the original publication's main text and supplementary material for a more thorough description of the algorithm. A schematic representation of the algorithm's architecture is shown in **Fig.S4**.

First, an initial seed network is selected by the user as the starting point of the evolution simulation. φ-evo then clones this first individual to create a population of networks. At each epoch, mutations are randomly applied to the networks of the population. Those mutations vary from topological changes to the network, where biochemical species or interactions can be added or removed, to non-topological changes, where the networks' kinetic parameter values are modified. Following mutations, networks are ranked based on their performance at accomplishing the biological function we select for. This performance is encoded via a user-defined fitness function that is problem specific. We give details about the specific implementation of the fitness functions for cell size control in the following subsection. After ranking the networks, φ-evo proceeds to select the most fit half of the network population. The less fit half is then discarded and replaced by a copy of the most fit half to maintain a constant population size. With this, φ-evo completes the first epoch of the evolutionary process. We use the term 'epoch' here rather than the term 'generation' which we retain to describe a cell lineage. A predetermined number of epochs of mutation and selection are then performed after which a final population of networks is extracted.

A. Fitness

In order to rank and select networks based on their performance at accomplishing a specific biological function, we design a specific objective function that we call <u>fitness</u>. Here, we chose a fitness function that could quantify a model's ability to produce many viable descendants during a fixed time period of length t. We initially considered a simple fitness function to be minimized by φ-evo, $f_0 = -N_{Div}$. Here N_{Div} is the number of divisions or *generations* in a cell lineage produced

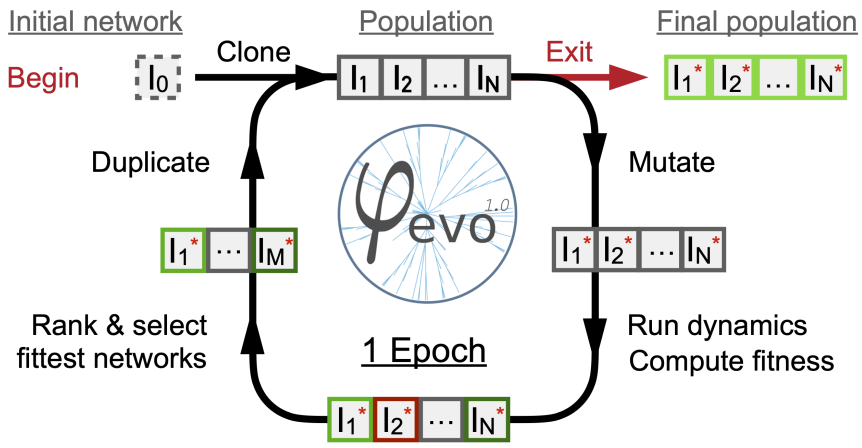

Fig. S4. Schematic representation of the φ-evo algorithm.
We begin with a user-defined initial seed network as starting point of the evolutionary process. The seed network is cloned to give a first population of networks. Individuals are then mutated randomly given the mutation parameters of the run. The dynamics and fitness scores of the networks are then computed and ranked. The best half of the population is selected and retained and the rest are discarded. The best half is then duplicated to maintain a constant population size N. We then repeat these instructions for a predefined number of epochs, after which a final population of networks is extracted and analyzed.

during a total time period of length t. Noise at the G1/S transition and in the S/G2/M timer duration act as a source of variation in volume at each generation which needs to be controlled by the evolved networks in order to prevent the cell volumes from diverging. Thus, networks that perform size control display a high number of divisions N_{Div}. The cycle duration distribution of a size control network will be centered around the doubling time τ in order to promote stable growth. Thus, on average, we expect a fit network to exhibit a maximum number of $\max(N_{Div}) = t/\tau$ divisions during a simulation of length t. Note that this number is mostly independent of the volume range selected by the evolutionary simulation as the doubling time τ is independent of the initial volume of the cell at the beginning of each cycle. There is a small effect on N_{Div} from the initial conditions chosen for the system of ODEs modelling the cell cycle, but this effect is mostly negligible as long as the total time period $t \gg \tau$.

In our first evolution experiments, we found that the single objective function $f_0 = -N_{Div}$ was insufficient alone to evolve a cycling network. A possible reason for this is that the fitness landscape in parameter space defined by f_0 is mostly flat far from the optimum and is difficult to navigate as it doesn't incrementally guide the evolution process towards a proper size control phenotype. Indeed, a network that does not perform size control will display very few divisions before diverging towards sizes of 0 or ∞. In contrast, a network that *does* performs some size control, even if performed badly, will display mostly stable growth with many divisions and the volume will not diverge over successive generations. There is thus an all or nothing effect with this fitness function. We found that optimization process would

often get stuck in a local optima with a low number of divisions and could not find a path to the global optima of size control. Because of this, we chose to turn towards multi-objective Pareto optimization which aims to simultaneously optimize several fitness functions. The idea here is that an additional fitness function can guide the evolutionary process through a different path in parameter space and could allow the evolutionary procedure to escape local optima.

In the Pareto optimization framework, we consider N equally important objective functions $\vec{f} = (f_0, f_1, ..., f_N)$. Assuming that fitness functions are to be maximized, we say that individual i (strictly) dominates individual j if and only if their fitness $\vec{f}^{\,i}$ and $\vec{f}^{\,j}$ are such that:

$$\forall\ k \in \{1, N\}, f_k^i \geq f_k^j \text{ and } \exists\ k' \in \{1, N\} \mid f_{k'}^i > f_{k'}^j$$

The algorithm then selects half of the population of the highest rank using a fitness sharing algorithm to maximize population diversity. We refer the reader to [8] for more details on this procedure.

For this project, we chose to limit the optimization process to two fitness functions. We chose $f_0 = -N_{div}$ as the first fitness function. We tested different measures of size control for the second objective function which are described in the following subsections. In most of the cases, we chose the coefficient of variation of the size distribution at birth CV_{Birth} to be minimized as the second fitness function.

A.1. Residuals

We first tested a least squared residuals fitness function to be minimized by φ-evo. This function yielded successful evolutionary runs but was abandoned due to requiring a user-defined target volume V_t. Indeed, we wanted to avoid the bias where we could select for biochemical networks matching a specific volume range. We used the following equation for the fitness function with $V_{\text{Birth}}^{(n)}$ indicating the cell volume at birth at the n-th generation in a lineage.

$$f_1 = \frac{1}{N_{\text{Div}} V_0} \sqrt{\sum_{n=1}^{N_{\text{Div}}} (V_{\text{Birth}}^{(n)} - V_t)^2} \tag{S15}$$

A.2. Coefficient of variation

We then considered the coefficient of variation of the size distribution at birth (CV_{Birth}) to be minimized by φ-evo. The CV_{Birth} is a measure of size control that normalizes the variance of the size distribution at birth with respect to its mean and is thus mostly insensitive to the absolute volume range of the cell. We chose this second fitness function in most of the Pareto optimization evolution experiments as described in the main text.

$$f_2 = CV_{\text{Birth}} = \frac{\sqrt{\mathbf{Var}[V_{\text{Birth}}]}}{\mathbf{E}[V_{\text{Birth}}]} \tag{S16}$$

A.3. Added volume slope in G1

We also considered directly optimizing the fitted slope of the volume added in G1 as a function of volume at birth to reinforce the sizer behavior in G1. As described

in the main text, given a series of volume values at birth and at G1/S, $V_{\text{Birth}}^{(i)}$ and $V_{\text{G1/S}}^{(i)}$ for $i \in \{1, N_{\text{Div}}\}$, the added volumes in G1 are defined as:

$$\Delta V_{\text{G1}}^{(i)} = V_{\text{G1/S}}^{(i)} - V_{\text{Birth}}^{(i)}$$

The best fit slope m of a linear model $\Delta V_{\text{G1}} = m \cdot V_{\text{Birth}} + b$ has a closed-form equation which is given as a function of the lineage data directly:

$$m = \frac{N_{\text{Div}} \cdot \left(\sum_{i=1}^{N_{\text{Div}}} V_{\text{Birth}}^{(i)} \cdot \Delta V_{\text{G1}}^{(i)} \right) - \left(\sum_{i=1}^{N_{\text{Div}}} V_{\text{Birth}}^{(i)} \right) \cdot \left(\sum_{i=1}^{N_{\text{Div}}} \Delta V_{\text{G1}}^{(i)} \right)}{N_{\text{Div}} \cdot \sum_{i=1}^{N_{\text{Div}}} \left(V_{\text{Birth}}^{(i)} \right)^2 - \left(\sum_{i=1}^{N_{\text{Div}}} V_{\text{Birth}}^{(i)} \right)^2} \tag{S17}$$

A slope of -1 corresponds to a sizer, a slope of 0 to an adder and a slope of +1 corresponds to a timer. In order to directly optimize the size control mechanism in G1 and to bias towards sizer mechanisms and to keep the fitness values positive, we considered the following fitness function to be minimized by φ-evo:

$$f_3 = m + 1 \tag{S18}$$

B. Biochemical interactions

In this project, we restricted the biochemical interactions available for evolution to transcriptional activation and repression, complexation also known as protein-protein interaction (PPI) and passive degradation. The equations for these interactions are presented in this subsection.

We model transcriptional activation of arbitrary network species **Y**'s production from species **X** using the following Hill equation:

$$\text{Activation}_{X \to Y}([\mathbf{X}], t_{X:Y}, n_{X:Y}) = \frac{([\mathbf{X}]/t_{X:Y})^{n_{X:Y}}}{1 + ([\mathbf{X}]/t_{X:Y})^{n_{X:Y}}} \tag{S19}$$

Similarly, repression of arbitrary species **Y**'s production from species **X** is modeled via the following Hill equation:

$$\text{Repression}_{X \to Y}([\mathbf{X}], t_{X:Y}, n_{X:Y}) = \frac{1}{1 + ([\mathbf{X}]/t_{X:Y})^{n_{X:Y}}} \tag{S20}$$

In these equations, $t_{X:Y}$ is the threshold required for $[\mathbf{X}]$ to activate or repress $[\mathbf{Y}]$ at 50% of its capacity and $n_{X:Y}$ is the Hill coefficient. While both types of interactions are modeled using Hill equations, their combined effects on a network species' dynamics is computed differently. Indeed, only the maximum of all the activations is accounted for whereas the inhibitions are multiplicative and all are accounted for. Additionally, we allow some species to be produced at a basal rate b independent of any activator which counts as an additional activation.

Altogether using an example, assuming multiple species $\mathbf{X}_1, ..., \mathbf{X}_q$ activate the production of species **Z** while multiples species $\mathbf{Y}_1, ..., \mathbf{Y}_r$ repress it, and assuming that **Z** has a basal production rate b_Z and a maximum production rate p_Z, then the total contribution of these interactions to the ODE for the dynamics of $[\mathbf{Z}]$ is given by:

$$\frac{d[\mathbf{Z}]}{dt} = \max\left[p_Z \cdot \max\left[\frac{([\mathbf{X}_1]/t_{X_1:Z})^{n_{X_1:Z}}}{1+([\mathbf{X}_1]/t_{X_1:Z})^{n_{X_1:Z}}}, \dots, \frac{([\mathbf{X}_q]/t_{X_q:Z})^{n_{X_q:Z}}}{1+([\mathbf{X}_q]/t_{X_q:Z})^{n_{X_q:Z}}}\right], b_Z\right] \cdot \prod_{i=1}^{r} \frac{1}{1+([\mathbf{Y}_i]/t_{Y_i:Z})^{n_{Y_i:Z}}} \tag{S21}$$

We use the law of mass-action to model PPIs and passive degradation. Specifically, if arbitrary species **X** and **Y** interact together and form a complex **Z** given a forward rate k_f and a backwards rate k_b, then the contribution of these interactions to the ODE for the dynamics of the system will be given by:

$$\frac{d[\mathbf{X}]}{dt} = \frac{d[\mathbf{Y}]}{dt} = -\frac{d[\mathbf{Z}]}{dt} = -k_f[\mathbf{X}] \cdot [\mathbf{Y}] + k_b[\mathbf{Z}] \tag{S22}$$

Lastly, all network species are assumed to be degraded at a passive rate. Thus, if an arbitrary species **X** is solely degraded with a rate δ_X, then the dynamic equation for the dynamics of $[\mathbf{X}]$ will be given by:

$$\frac{d[\mathbf{X}]}{dt} = -\delta_X[\mathbf{X}] \tag{S23}$$

4. MODEL DESCRIPTIONS

In this section, we give the full set of equations and parameter values of the models from the main text.

Model A1

The parameter values of the Model A1 are shown in Table S1 along with the corresponding differential equations in eq. S24.

Table S1. Model A1 parameter values

Parameter	Value	Parameter	Value
p_2	0.369408	δ_3	0.4574764
$t_{1:2}$	1.104619	k_{f1}	6.783001
$n_{1:2}$	3.215727	k_{b1}	0.195168
δ_2	0.083827	δ_4	4.244007
p_3	0.703658	k_{f2}	0.021174
$t_{2:3}$	0.044938	k_{b2}	1.075146
$n_{2:3}$	3.266732	δ_5	1.1010876

$$
\begin{aligned}
\frac{d[\mathbf{I}]}{dt} &= p_2 \frac{(\textbf{S/G2/M Switch}/t_{1:2})^{n_{1:2}}}{1+(\textbf{S/G2/M Switch}/t_{1:2})^{n_{1:2}}} - k_{f1}[\mathbf{I}]\cdot[\mathbf{R}] + k_{b1}[\mathbf{S}_4] - k_{f2}[\mathbf{I}]^2 + k_{b2}[\mathbf{S}_5] \\
&\quad - (\delta_2+\lambda)[\mathbf{I}] \\
\frac{d[\mathbf{R}]}{dt} &= p_3 \frac{1}{1+([\mathbf{I}]/t_{2:3})^{n_{2:3}}} - k_{f1}[\mathbf{I}]\cdot[\mathbf{R}] + k_{b1}[\mathbf{S}_4] - (\delta_3+\lambda)[\mathbf{I}] \\
\frac{d[\mathbf{S}_4]}{dt} &= k_{f1}[\mathbf{I}]\cdot[\mathbf{R}] - k_{b1}[\mathbf{S}_4] - (\delta_4+\lambda)[\mathbf{S}_4] \\
\frac{d[\mathbf{S}_5]}{dt} &= k_{f2}[\mathbf{I}]^2 - k_{b2}[\mathbf{S}_5] - (\delta_5+\lambda)[\mathbf{S}_5]
\end{aligned}
\tag{S24}
$$

Model A2

The parameter values of the Model A2 are shown in Table S2 along with the corresponding differential equations in eq. S25.

Table S2. Model A2 parameter values

Parameter	Value	Parameter	Value
p_2	1.915601	$n_{1:3}$	2.751652
$t_{1:2}$	0.178720	$t_{2:3}$	0.441106
$n_{1:2}$	2.090540	$n_{2:3}$	2.780297
$t_{3:2}$	0.962612	δ_3	0.045051
$n_{3:2}$	2.144666	k_{f1}	0.839879
δ_2	0.019495	k_{b1}	0.381067
p_3	1.944803	δ_4	0.913992
$t_{1:3}$	0.422939		

$$
\begin{aligned}
\frac{d[\mathbf{I}]}{dt} &= p_2 \frac{(\textbf{S/G2/M Switch}/t_{1:2})^{n_{1:2}}}{1+(\textbf{S/G2/M Switch}/t_{1:2})^{n_{1:2}}} \frac{1}{1+([\mathbf{R}]/t_{3:2})^{n_{3:2}}} - k_{f1}[\mathbf{I}]\cdot[\mathbf{R}] + k_{b1}[\mathbf{S}_4] \\
&\quad - k_{f2}[\mathbf{I}]^2 + k_{b2}[\mathbf{S}_5] - (\delta_2+\lambda)[\mathbf{I}] \\
\frac{d[\mathbf{R}]}{dt} &= p_3 \frac{1}{1+([\mathbf{I}]/t_{2:3})^{n_{2:3}}} \frac{1}{1+(\textbf{S/G2/M Switch}/t_{1:3})^{n_{1:3}}} - k_{f1}[\mathbf{I}]\cdot[\mathbf{R}] + k_{b1}[\mathbf{S}_4] \\
&\quad - (\delta_3+\lambda)[\mathbf{I}] \\
\frac{d[\mathbf{S}_4]}{dt} &= k_{f1}[\mathbf{I}]\cdot[\mathbf{R}] - k_{b1}[\mathbf{S}_4] - (\delta_4+\lambda)[\mathbf{S}_4]
\end{aligned}
\tag{S25}
$$

Model B

The parameter values of the fluctuation-sensing Model B are shown in Table S3 along with the corresponding stochastic differential equations in eq. S26. We note

that the C_0 parameter in the noise terms of the equation is a concentration scaling factor.

Table S3. Model B parameter values

Parameter	Value	Parameter	Value
p_2	4.968896	$n_{3:3}$	3.189190
$t_{1:2}$	2.569361	δ_3	0.246561
$n_{1:2}$	0.952178	p_4	4.674459
$t_{3:2}$	0.131057	δ_4	1.010978
$n_{3:2}$	9.219961	k_f	3.194116
δ_2	0.521437	k_b	4.634009
p_3	0.113586	δ_5	1.165439
$t_{3:3}$	2.183079	C_0	1

$$
\begin{aligned}
\frac{d[\mathbf{I}]}{dt} &= p_2 \cdot \max\left(\frac{(\textbf{S/G2/M Switch}/t_{1:2})^{n_{1:2}}}{1+(\textbf{S/G2/M Switch}/t_{1:2})^{n_{1:2}}}, \frac{([\mathbf{A}]/t_{3:2})^{n_{3:2}}}{1+([\mathbf{A}]/t_{3:2})^{n_{3:2}}}\right) - (\delta_2+\lambda)[\mathbf{I}] \\
&\quad + \mathcal{N}_1(0,1) \cdot \sqrt{\frac{p_2 \cdot \max\left(\frac{(\textbf{S/G2/M Switch}/t_{1:2})^{n_{1:2}}}{1+(\textbf{S/G2/M Switch}/t_{1:2})^{n_{1:2}}}, \frac{([\mathbf{A}]/t_{3:2})^{n_{3:2}}}{1+([\mathbf{A}]/t_{3:2})^{n_{3:2}}}\right) + \delta_2[\mathbf{I}]}{V \cdot C_0 \cdot \Delta t}} \\
\frac{d[\mathbf{A}]}{dt} &= p_3 \cdot \frac{([\mathbf{A}]/t_{3:3})^{n_{3:3}}}{1+([\mathbf{A}]/t_{3:3})^{n_{3:3}}} - k_f[\mathbf{A}]\cdot[\mathbf{S}_4] + k_b[\mathbf{S}_5] - (\delta_3+\lambda)[\mathbf{I}] \\
&\quad + \mathcal{N}_2(0,1) \cdot \sqrt{\frac{p_3 \cdot \frac{([\mathbf{A}]/t_{3:3})^{n_{3:3}}}{1+([\mathbf{A}]/t_{3:3})^{n_{3:3}}} + \delta_3[\mathbf{A}]}{V \cdot C_0 \cdot \Delta t}} - \mathcal{N}_3(0,1) \cdot \sqrt{\frac{k_f[\mathbf{A}]\cdot[\mathbf{S}_4]}{V \cdot C_0 \cdot \Delta t}} \\
&\quad + \mathcal{N}_4(0,1) \cdot \sqrt{\frac{k_b[\mathbf{S}_5]}{V \cdot C_0 \cdot \Delta t}} \\
\frac{d[\mathbf{S}_4]}{dt} &= p_4 - k_f[\mathbf{A}]\cdot[\mathbf{S}_4] + k_b[\mathbf{S}_5] - (\delta_4+\lambda)[\mathbf{S}_4] - \mathcal{N}_3(0,1) \cdot \sqrt{\frac{k_f[\mathbf{A}]\cdot[\mathbf{S}_4]}{V \cdot C_0 \cdot \Delta t}} \\
&\quad + \mathcal{N}_4(0,1) \cdot \sqrt{\frac{k_b[\mathbf{S}_5]}{V \cdot C_0 \cdot \Delta t}} + \mathcal{N}_5(0,1) \cdot \sqrt{\frac{p_4 + \delta_4[\mathbf{S}_4]}{V \cdot C_0 \cdot \Delta t}} \\
\frac{d[\mathbf{S}_5]}{dt} &= k_f[\mathbf{A}]\cdot[\mathbf{S}_4] - k_b[\mathbf{S}_5] - (\delta_5+\lambda)[\mathbf{S}_5] + \mathcal{N}_3(0,1) \cdot \sqrt{\frac{k_f[\mathbf{A}]\cdot[\mathbf{S}_4]}{V \cdot C_0 \cdot \Delta t}} \\
&\quad - \mathcal{N}_4(0,1) \cdot \sqrt{\frac{k_b[\mathbf{S}_5]}{V \cdot C_0 \cdot \Delta t}} + \mathcal{N}_6(0,1) \cdot \sqrt{\frac{\delta_5[\mathbf{S}_5]}{V \cdot C_0 \cdot \Delta t}}
\end{aligned}
\tag{S26}
$$

5. ADDITIONAL MODELS

Here we present additional models that were evolved but not discussed in the main text to provide more examples of size control mechanisms.

Model A3

Model A3 is similar to Model A1, but lacks the homodimerization interaction of **I** (see eq. S24). This specific model results in a weak adder/timer that displays a non-linear size control response curve. This is similar to Model A2 where we see a sizer/adder behavior in the low control volume regime and adder/timer behavior in the high control volume regime.

This model's behavior is summarized in **Fig.S5**. The parameter values of the model are shown in Table S4 along with the corresponding differential equations in eq. S27. This model was evolved with the Pareto fitness optimization framework to maximize N_{Div} and minimize CV_{Birth}. The initial seed model topology for this evolutionary simulation was the quantity sensing oscillator shown in **Fig.S3A** and was optimized during 3000 epochs.

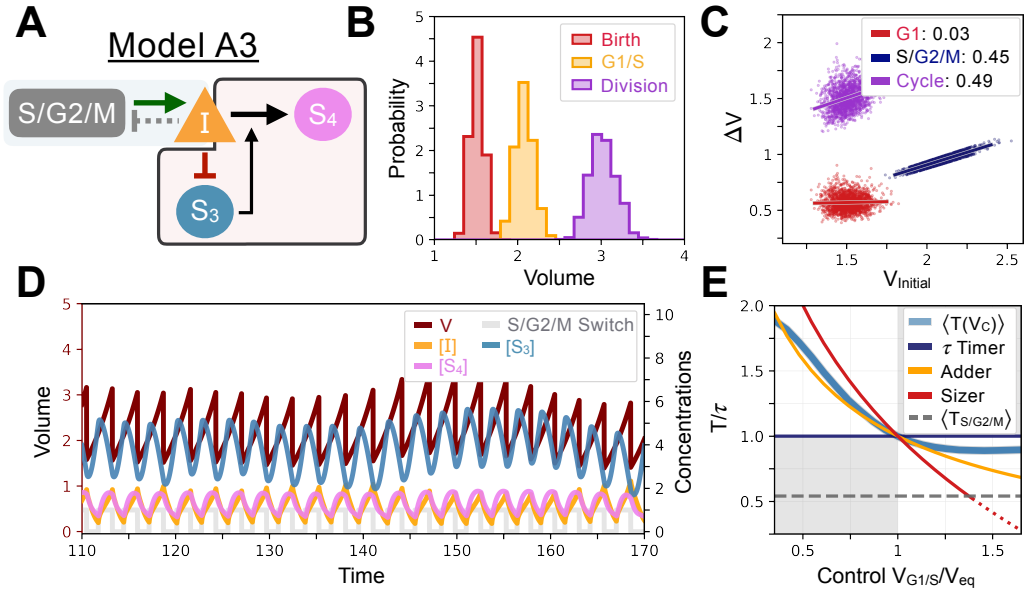

Fig. S5. Model A3's behavior.
A - Network topology of the evolved Model A3. S_3 is as a size sensor and titrates I in a size-dependent manner. **B** Size distributions at birth (red), G1/S (orange), and division (purple). **C** Added volumes in G1 (red), S/G2/M (blue) and over the whole cycle (purple) as a function of the volume at the beginning of those phases. **D** Temporal dynamics of the model, colors correspond to the variables in **A**. **E** Response curve $T(V_C)$ as a function of control volume V_C at the G1/S transition.

Table S4. Model A3 parameter values

Parameter	Value	Parameter	Value
p_2	5.606156	$t_{2:3}$	1.410420
$t_{1:2}$	0.066136	$n_{2:3}$	3.434213
$n_{1:2}$	8.177965	k_f	1.930909
b_2	0.911279	k_b	3.871610
δ_2	0.257920	δ_3	0.013294
p_3	5.887584	δ_4	1.803926

$$
\begin{aligned}
\frac{d[\mathbf{I}]}{dt} &= \max\left(p_2 \cdot \frac{(\textbf{S/G2/M Switch}/t_{1:2})^{n_{1:2}}}{1+(\textbf{S/G2/M Switch}/t_{1:2})^{n_{1:2}}}, b_2\right) - k_f[\mathbf{I}]\cdot[\mathbf{S}_3] + k_b[\mathbf{S}_4] \\
&\quad - (\delta_2+\lambda)[\mathbf{I}] \\
\frac{d[\mathbf{S}_3]}{dt} &= \frac{p_3}{1+(\mathbf{I}/t_{2:3})^{n_{2:3}}} - k_f[\mathbf{I}]\cdot[\mathbf{S}_3] + k_b[\mathbf{S}_4] - (\delta_3+\lambda)[\mathbf{S}_3] \\
\frac{d[\mathbf{S}_4]}{dt} &= k_f[\mathbf{I}]\cdot[\mathbf{S}_3] - k_b[\mathbf{S}_4] - (\delta_4+\lambda)[\mathbf{S}_4]
\end{aligned}
\tag{S27}
$$

Model A4

Model A4 is similar in essence to Model A1, albeit more unstable. In this model, $\mathbf{S}_4$ is the size sensor. Instead of using a PPI to titrate **I** in a size-dependent manner in G1, this model leverages a transcriptional repression to modulate the production of **I** directly rather than its effective degradation. The model's behavior is summarized in **Fig.S6**. The parameter values of the model are shown in Table S5 along with the corresponding differential equations in eq. S28. Notably, Fig. S6 - **E** shows that the model's response curve in the low control volume regime is ill-defined. In practice, due to intrinsic noise at the G1/S transition and in the S/G2/M timer length, we've seen a cell lineage terminate prematurely before it can reach the maximum number of N_{Div} allowed in a simulation. One could say this model is thus less fit than those presented in the main text, although it displays an added volume slope over its cycle of -0.41 and is close to a sizer.

This model was evolved using a Pareto fitness optimization that maximizes N_{Div} and minimizes CV_{Birth}. The initial model topology was the quantity sensing oscillator of **Fig.S3A** which was optimized over 4000 epochs.

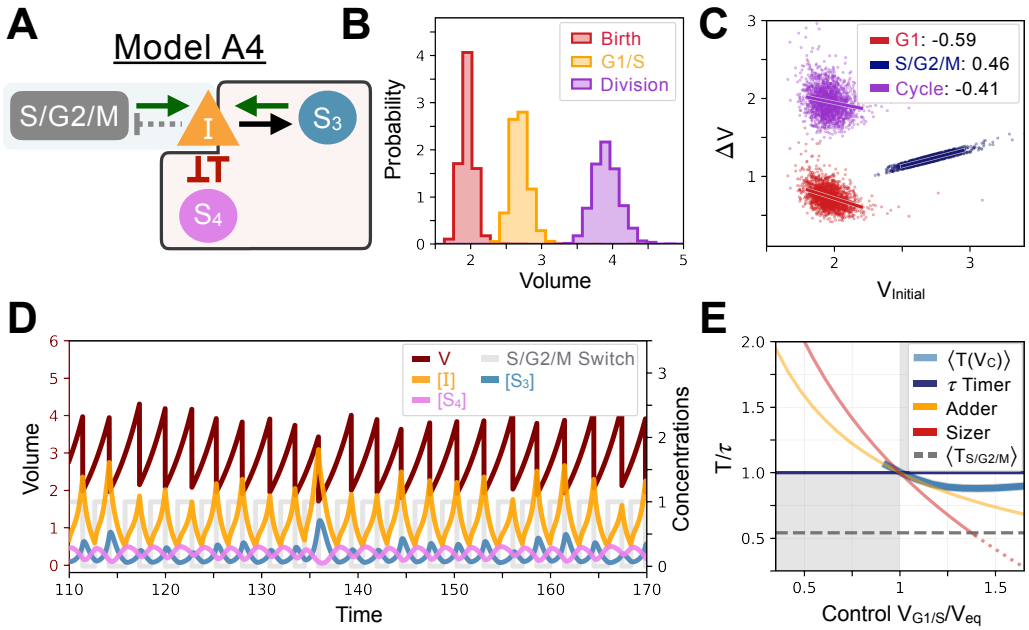

Fig. S6. Model A4's behavior.
A - Network topology of the evolved Model 3. S_4 is the size sensor and represses the production of I in a size-dependent manner. **B** Size distributions at birth (red), G1/S (orange) and division (purple). **C** Added volumes in G1 (red), S/G2/M (blue) and over the whole cycle (purple) as a function of initial volume at the start of those phases. **D** Temporal dynamics of the model, colors correspond to the variables in **A**. **E** Response curve $T(V_C)$ as a function of control volume V_C at the G1/S transition.

Table S5. Model A4 parameter values

Parameter	Value	Parameter	Value
p_2	5.6604334	δ_2	0.001059
$t_{1:2}$	0.408208	k_f	0.843408
$n_{1:2}$	1.769233	k_b	1.680321
$t_{3:2}$	0.887392	δ_3	0.825150
$n_{3:2}$	6.437683	p_4	4.674459
$t_{4:2}$	0.197495	$t_{2:4}$	0.744119
$n_{4:2}$	3.238633	$n_{2:4}$	3.451469
b_2	0.800255	δ_4	1.929584

$$
\begin{aligned}
\frac{d[\mathbf{I}]}{dt} &= \max\left(p_2 \cdot \max\left(\frac{(\textbf{S/G2/M Switch}/t_{1:2})^{n_{1:2}}}{1+(\textbf{S/G2/M Switch}/t_{1:2})^{n_{1:2}}}, \frac{([\mathbf{S}_3]/t_{3:2})^{n_{3:2}}}{1+([\mathbf{S}_3]/t_{3:2})^{n_{3:2}}}\right), b_2\right) \\
&\quad \cdot \frac{1}{1+(\mathbf{S}_4/t_{4:2})^{n_{4:2}}} - k_f[\mathbf{I}]^2 + k_b[\mathbf{S}_3] - (\delta_2+\lambda)[\mathbf{I}] \\
\frac{d[\mathbf{S}_3]}{dt} &= k_f[\mathbf{I}]^2 - k_b[\mathbf{S}_3] - (\delta_3+\lambda)[\mathbf{S}_3] \\
\frac{d[\mathbf{S}_4]}{dt} &= \frac{p_4}{1+(\mathbf{I}/t_{2:4})^{n_{2:4}}} - (\delta_4+\lambda)[\mathbf{S}_4]
\end{aligned}
\tag{S28}
$$

Model A5

Model A5 is another variation on Model A1 but here within the *S. pombe* cell cycle framework where I controls the timing of division directly and the Switch is turned on in G1 instead of S/G2/M. Here, $\mathbf{S}_3$ directly senses size and does so via the PPI linking $\mathbf{I}$, $\mathbf{S}_3$, and $\mathbf{S}_7$. Indeed, since $\mathbf{I}$ is inversely proportional to the volume at G1/S due to quantity sensing and since $\mathbf{S}_7$ is solely produced via complex formation of $\mathbf{I}$ with $\mathbf{S}_3$, $\mathbf{S}_7$ is also inversely proportional to volume. Consequently, $\mathbf{S}_3$, which is almost solely produced via the dissociation of $\mathbf{S}_7$, becomes a direct sensor of the size of the cell.

Then, instead of using a PPI to titrate $\mathbf{I}$ in a size-dependent manner as is done in Models A1 and A2, Model A5 leverages a transcriptional repression mechanism to modulate the production of $\mathbf{I}$ directly instead of its degradation, precisely like in Model A4. The model's behavior is summarized in **Fig.S7**. The parameter values of the model are shown in Table S6 along with the corresponding differential equations in eq. S29.

This model was evolved using a Pareto fitness optimization that mazimizes N_{Div} and minimizes CV_{Birth}. The seed model topology was the quantity sensing oscillator of **Fig.S3A** which was optimized over 2500 epochs.

$$
\begin{aligned}
\frac{d[\mathbf{I}]}{dt} &= p_2 \cdot \max\left(\frac{(\textbf{G1 Switch}/t_{1:2})^{n_{1:2}}}{1+(\textbf{G1 Switch}/t_{1:2})^{n_{1:2}}}, b_2\right) \cdot \frac{1}{1+(\mathbf{S}_3/t_{3:2})^{n_{3:2}}} \cdot \frac{1}{1+(\mathbf{S}_4/t_{4:2})^{n_{4:2}}} \\
&\quad - k_{f1}[\mathbf{I}]\cdot[\mathbf{S}_4] + k_{b1}[\mathbf{S}_6] - k_{f2}[\mathbf{I}]^2 + k_{b2}[\mathbf{S}_5] - k_{f3}[\mathbf{I}]\cdot[\mathbf{S}_3] + k_{b3}[\mathbf{S}_7] \\
&\quad - (\delta_2+\lambda)[\mathbf{I}] \\
\frac{d[\mathbf{S}_3]}{dt} &= b_3 - k_{f3}[\mathbf{I}]\cdot[\mathbf{S}_3] + k_{b3}[\mathbf{S}_7] - (\delta_3+\lambda)[\mathbf{S}_3] \\
\frac{d[\mathbf{S}_4]}{dt} &= b_4 - k_{f1}[\mathbf{I}]\cdot[\mathbf{S}_4] + k_{b1}[\mathbf{S}_6] - (\delta_4+\lambda)[\mathbf{S}_4] \\
\frac{d[\mathbf{S}_5]}{dt} &= k_{f2}[\mathbf{I}]^2 - k_{b2}[\mathbf{S}_5] - (\delta_5+\lambda)[\mathbf{S}_5] \\
\frac{d[\mathbf{S}_6]}{dt} &= k_{f1}[\mathbf{I}]\cdot[\mathbf{S}_4] - k_{b1}[\mathbf{S}_6] - (\delta_6+\lambda)[\mathbf{S}_6] \\
\frac{d[\mathbf{S}_7]}{dt} &= k_{f3}[\mathbf{I}]\cdot[\mathbf{S}_3] - k_{b3}[\mathbf{S}_7] - (\delta_7+\lambda)[\mathbf{S}_7]
\end{aligned}
\tag{S29}
$$

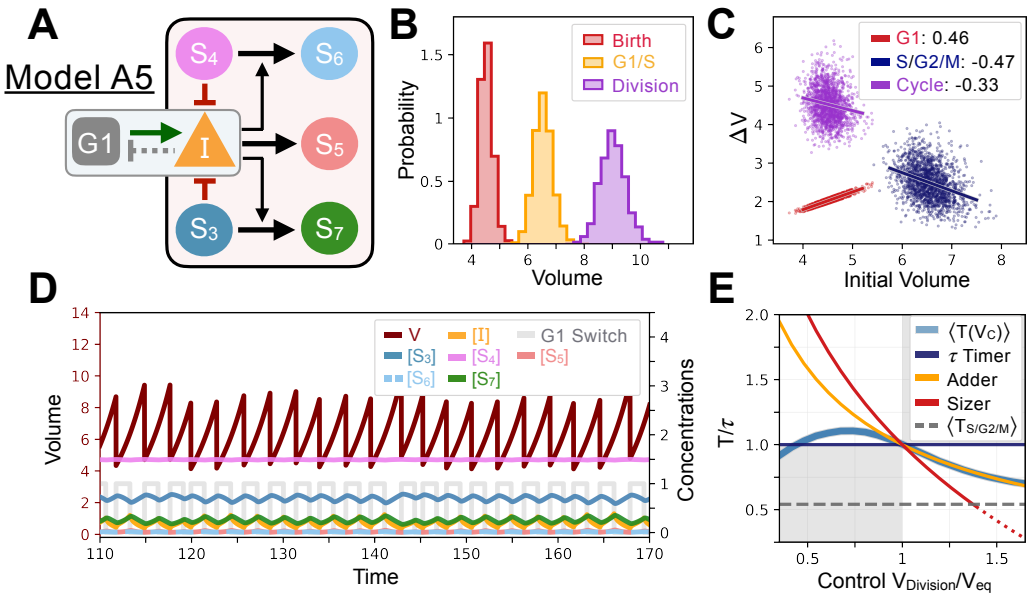

Fig. S7. Model A5's behavior.
A - Network topology of the evolved Model A5. S_3 is the size sensor and represses the production of I in a size-dependent manner. **B** Size distributions at birth (red), G1/S (orange) and division (purple). **C** Added volumes in G1 (red), S/G2/M (blue) and over the whole cycle (purple) as a function of initial volume at the start of those phases. **D** Temporal dynamics of the model, colors correspond to the variables in **A**. **E** Response curve $T(V_C)$ as a function of control volume V_C at division.

Table S6. Model A5 parameter values

Parameter	Value	Parameter	Value
p_2	2.379635	b_4	2.624939
$t_{1:2}$	0.142770	δ_4	1.499653
$n_{1:2}$	0.383384	δ_5	0.006318
$t_{3:2}$	0.714386	δ_6	0.983140
$n_{3:2}$	8.642875	δ_7	0.481592
$t_{4:2}$	1.754776	k_{f1}	0.226150
$n_{4:2}$	7.783080	k_{b1}	3.793388
b_2	0.195855	k_{f2}	1.608325
δ_2	0.576282	k_{b2}	3.322565
b_3	0.582449	k_{f3}	2.999118
δ_3	0.318466	k_{b3}	0.906997

REFERENCES

1. Y. Chen, G. Zhao, J. Zahumensky, S. Honey, and B. Futcher, "Differential scaling of gene expression with cell size may explain size control in budding yeast," Mol. cell **78**, 359–370.e6 (2020).
2. M. P. Swaffer, J. Kim, D. Chandler-Brown, M. Langhinrichs, G. K. Marinov, W. J. Greenleaf, A. Kundaje, K. M. Schmoller, and J. M. Skotheim, "Transcriptional and chromatin-based partitioning mechanisms uncouple protein scaling from cell size," Mol. Cell **81**, 4861–4875.e7 (2021).
3. J. R. S. Newman, S. Ghaemmaghami, J. Ihmels, D. K. Breslow, M. Noble, J. L. DeRisi, and J. S. Weissman, "Single-cell proteomic analysis of S. cerevisiae reveals the architecture of biological noise," Nature **441** (2006).
4. D. T. Gillespie, "Stochastic simulation of chemical kinetics," Annu. Rev. Phys. Chem. **58**, 35–55 (2007).
5. P. E. Kloeden and E. Platen, *Numerical solution of stochastic differential equations* (Springer-Verlag Berlin ; New York, 1992).
6. K. M. Schmoller, J. J. Turner, M. Kõivomägi, and J. M. Skotheim, "Dilution of the cell cycle inhibitor Whi5 controls budding-yeast cell size," Nature **526** (2015).
7. A. Henry, M. Hemery, and P. Francois, "φ-evo : A program to evolve phenotypic models of biological networks," PLoS Comput. Biol. pp. 1–12 (2018).
8. A. Warmflash, P. Francois, and E. D. Siggia, "Pareto evolution of gene networks: an algorithm to optimize multiple fitness objectives," Phys. Biol. **9**, 056001 (2012).